

Gravitational wave signal of the short rise fling of galactic run away pulsars

ACCEPTED FOR PUBLICATION IN JCAP 17/10/2008

Herman J. Mosquera Cuesta^{1,2}, Carlos A. Bonilla Quintero¹

¹*Instituto de Cosmologia, Relatividade e Astrofísica (ICRA-BR), Centro Brasileiro de Pesquisas Físicas
Rua Dr. Xavier Sigaud 150, CEP 22290-180, Urca Rio de Janeiro, RJ, Brazil **

(Dated: August 25, 2021)

Determination of pulsar parallaxes and proper motions addresses fundamental astrophysical open issues. Here, after scrutinizing the ATNF Catalog searching for pulsar distances and proper motions, we verify that for an ATNF sample of 212 Galactic run away pulsars (RAPs), which currently run across the Galaxy at very high speed and undergo large displacements, some gravitational-wave (GW) signals produced by such present accelerations appear to be detectable after calibration against the Advanced LIGO (LIGO II). Motivated by this insight, we address the issue of the pulsar kick at birth, or *short rise fling* from a supernova explosion, by adapting the theory for emission of GW by ultrarelativistic sources to this case in which Lorentz factor is $\gamma \sim 1$. We show that during the short rise fling each run away pulsar (RAP) generates a GW signal with characteristic amplitude and frequency that makes it detectable by current GW interferometers. For a realistic analysis, an efficiency parameter is introduced to quantify the expenditure of the rise fling kinetic energy, which is estimated from the linear momentum conservation law applied to the supernova explosion that kicks out the pulsar. The remaining energy is supposed to be used to make the star to spin. Thus, a comparison with the spin of ATNF pulsars having velocity in the interval 400 – 500 km s⁻¹ is performed. The resulting difference suggests that other mechanisms (like differential rotation, magnetic breaking or magneto-rotational instability) should dissipate part of that energy to produce the observed pulsar spin periods. Meanwhile, the kick phenomenon may also occur in globular and open star clusters at the formation or disruption of very short period compact binary systems wherein abrupt velocity and acceleration similar to those given to RAPs during the short rise fling can be imparted to each orbital partner. To better analyzing these cases, pulsar astrometry from micro- to nano-arcsec scales might be of much help. In case of a supernova, the RAP GW signal could be a benchmark for the GW signal from the core collapse.

PACS numbers: 04.30.Db, 04.80.Nn, 97.60.Gb

I. ASTROPHYSICAL MOTIVATION

The detection of gravitational waves (GW) is one of the greatest goals of today's relativistic astrophysics. Because of the great success of Einstein's general relativity (GR) in explaining the dynamical evolution of the binary pulsar PSR 1913+16; continuously observed over almost 30 years by Taylor and Hulse [14], most researchers in the field are confident that the very first GW signal to be detected must come from coalescing binary neutron star-neutron star or black hole-neutron star (NS-NS, BH-NS) systems. Ongoing LIGO science runs [11] for the first time have set firm upper limits on the rate of binary coalescences in our Galaxy: at the level of a few events per year. Meanwhile the model-dependent estimate of such a rate at cosmic distance scales varies around 10⁻⁵ [12, 13, 21]. The expectation is enormous as well for an event like the supernova (SN) explosion.

In this paper we focus on the radiation emitted when a pulsar is kicked out from the supernova remnant and is accelerated with very high speed, albeit non ultrarelativistic. Gravitational radiation is emitted whenever the nascent neutron star or pulsar changes its

velocity, a condition that is fulfilled by the large thrust given to the nascent pulsar during the SN explosion, and also due to the pulsar dragging against the SN ejecta. (Recall that the gravitational field generated by a motion with constant velocity is nonradiative). We shall show that each individual event of launching a nascent pulsar to drift or run across the Galaxy, after a SN explosion, generates a gravitational wave signal that can be detected by current and planned GW interferometers such LIGO I, LIGO II, VIRGO, GEO-600, or TAMA-300. Nonetheless, it is stressed from the very beginning that the strain of the GW signal that we estimate below is a *lower bound*. The reason is that we are not taking into account the contribution to the GW amplitude, h , stemming from the effective acceleration that the pulsar receives at the kick at birth, which could be very large. Indeed, the distance over which the RAP is dragged against the supernova ejecta could also be astronomically large.

At first glance, it appears that the detection of the GW signal from the short rise must have an event rate on the order of that for SN events in our galaxy, i. e. ~ 1 per 30-300 years. In principle such a rate has to be the same because the flinging of the pulsar could be just the aftermath of most supernova core collapses. However, in galactic globular clusters, where the frequency of formation and disruption of binary systems harboring

*Electronic address: hermanjc@cbpf.br, herman@icra.it

compact stars is relatively high, the kick velocity of a pulsar partner at the binary disruption could be of the same magnitude as the one for galactic RAPs. Indeed, Vlemmings et al. [16] are pursuing a VLBI astrometry program to perform measurements of pulsar proper motions and parallaxes with spatial resolution of microarcsecond. As an illustration of the performance of the high precision pulsar astrometry system they simulated the detection of the disruption of a binary system in the stellar cluster Cygnus Superbubble. This is a quite stimulating perspective for pulsar astrometry in the near future.

Therefore, there is a potential to detect such a disruption or formation of a binary system through the GW signal emitted by the abrupt acceleration or sudden increase in velocity of a given pulsar. Observations in the range of micro- or nano-astrometry with planned satellites like GAIA and other instruments on Earth and space may help to identify such a phenomenon. An advanced technology useful for this purpose is currently operative or under planning (see Ref.[17] and references therein).

The physical reason for advocating in favor of this novel possibility for GW detection is based on a number of results on the dynamics and kinematics of galactic RAPs and also on GR, as is shown next.

- 1) In a seminal paper, Spruit and Phinney [5] demonstrated that regardless of the actual physical engine driving the natal (instantaneous) pulsar kicks, that mechanism can only act upon the pulsar over a very restricted time scale, $\Delta T_{\max}^{\text{kick}}$, on the order of $\simeq 0.32$ s. This is a fundamental piece of the dynamics of observed pulsars that seems to be overlooked by workers in the field.
- 2) As shown in the next Section, pulsar surveys have shown that the largest (V_{\star}^{\max}), smaller (V_{\star}^{\min}) and average (V_{\star}^{ave}) spatial (3-D) velocity of cataloged pulsars are 5000 km s^{-1} , 84 km s^{-1} , and $450\text{-}500 \text{ km s}^{-1}$, respectively [2, 4, 10] (see Fig.1(c)). That is, V_{\star} changes by more than an order of magnitude.
- 3) Observations of NSs in binary systems have allowed to estimate their masses with very high accuracy. The current values of this physical property gather around $1.4 M_{\odot}$ [8].
- 4) According to GR the acceleration of a mass (M_{\star}) to a relativistic velocity (V_{\star}); i. e. energy, should generate a GW pulse, the nature of which has a very distinctive imprint: the so-called gravitational wave memory [6, 18, 19], which makes the amplitude of this GW signal (the GW strain) not to fade away by the end of the traction phase (the kick), but rather leaves it variable in time as much as an energy source remains active in the source.

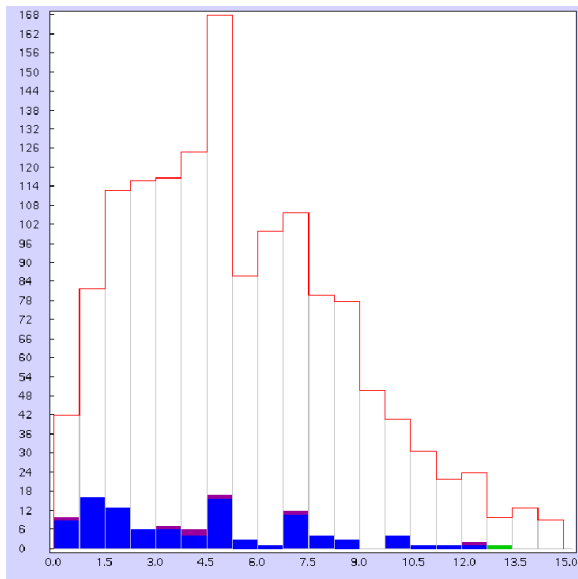
II. GALACTIC RAPs AND SAMPLE SELECTION FROM ATNF CATALOG

Run away pulsars (RAPs) are observed to drift along the Galaxy with velocities ranging from 90 km s^{-1} to 4000 km s^{-1} (Australian Telescope National Facility (ATNF) Catalog [1], [9]). Since most stars in our galaxy are observed to drift with average velocities of $15 - 30 \text{ km s}^{-1}$, it has been suggested that such large velocities should be given to the proto-neutron star at its birth. The kick velocity imparted to a just-born neutron star during the rise time is a fundamental piece for understanding the physics of the core collapse supernovae, to have an insight on the sources of asymmetries during the gravitational collapse and on the emission of gravitational waves during this process. There seems to be a consensus that the core collapse asymmetry driving the kick velocity of a neutron star at birth may have origin in a variety of mechanisms [25, 26].

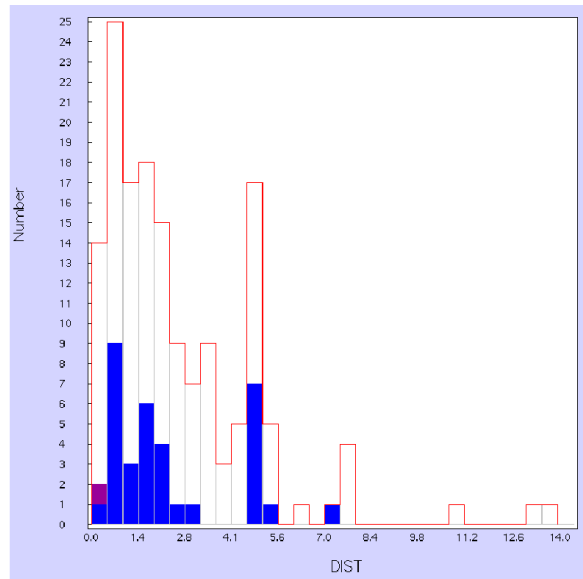
Although the mechanism responsible for the initial impulses has not been properly identified yet, a very strong constraint on the timescale over which it could act on the nascent neutron star (NS) was put forward in Ref.[5]. Whichever this thruster engine might be it cannot push the star over a timescale longer than $\Delta T_{\max}^{\text{kick}} \simeq 0.32$ s. Combining this with the NS mass, which piles-up around $1.4 M_{\odot}$ [8], and the above average velocity, implies that a huge power should be expended by the thruster during the pulsar early acceleration phase, and hereby a gravitational-wave (GW) burst with “memory” (understood as a steady time variation of the metric perturbation) must be released during this time, according to general relativity [6].

The present velocity distribution (see Figs.1, 1(c)) is constructed based on the analysis of the proper motion of radio pulsars in our Galaxy after estimating their distances. Pulsar distances are estimated by using annual parallax, H I absorption, or associations with globular clusters or supernova remnants, and from dispersion measures and galactic electron density models.

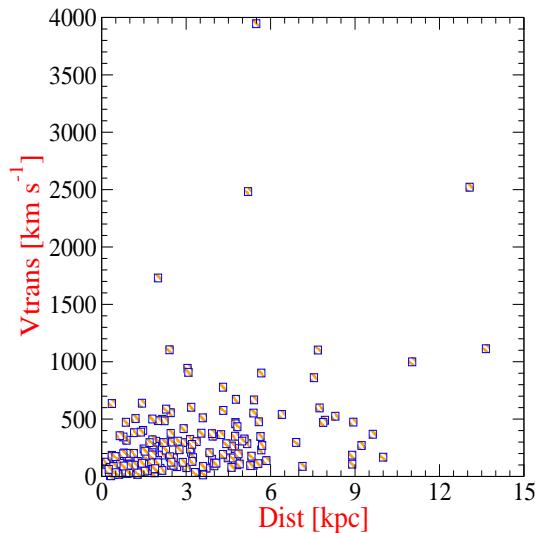
This astronomy field has become a vivid research enterprise since the pioneer works of Lyne and Lorimer (LL94) [2, 3]. However, the current view on the distribution of kick velocities is far from the original one they found through pulsar surveys fifteen years ago. LL94 showed that pulsars appear to run around the Galaxy (and its halo) with mean spatial (3-D) velocities $\sim 450 - 500 \text{ km s}^{-1}$ [2], but freeway (“cannon-ball”) pulsars with velocities as high as 5000 km s^{-1} and slow-down millisecond pulsars with speeds of 80 km s^{-1} wander also around the Galaxy [3]. Meanwhile, the situation changed dramatically with the pulsar velocity survey performed by Arzoumian, Chernoff and Cordes (ACC02) [4], who found that such a speed distribution appeared to be bimodal indicating one distribution mode around 90 km s^{-1} and another near 500 km s^{-1} . However, this dynamic research field has shown, through new studies on pulsar proper motions, that the situation



(a) Pulsar number (vertical axis) vs. distance (kpc) to Earth (horizontal axis) histogram



(b) Pulsar number vs. Distance distribution of 212 pulsars



(c) Velocity vs. Distance distribution of 212 ATNF pulsars having both parameters measured

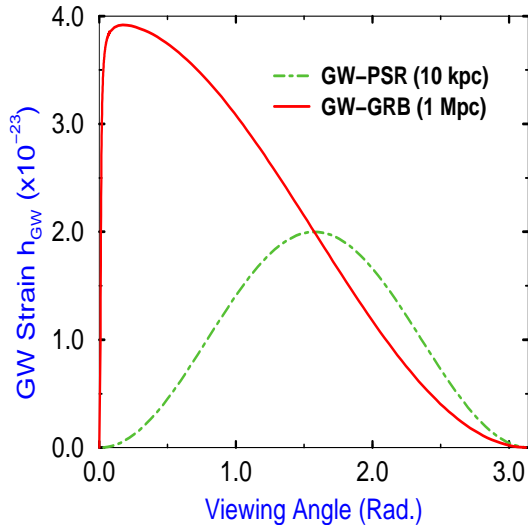
FIG. 1: Data taken from ATNF Pulsar Catalog

is far from having been settled. For instance, Hobbs et al. [10] have recently challenged the ACC02 findings, and have shown that their studies lead to assert that there is no evidence of a bimodal distribution. Instead they suggest that mean 3-Dim pulsar birth velocity is $400 \pm 40 \text{ km s}^{-1}$, and that the distribution appears to be Maxwellian with 1-Dim rms $\sigma = 265 \text{ km s}^{-1}$, showing also a continuum distribution from low to high (present) run away speeds, being the last ones the tail of the velocity distribution. Hence, looking back on the surveys by LL94, the study by Hobbs et al. [10] clearly agrees with the mean velocity of $450 \pm 90 \text{ km s}^{-1}$ found by LL94 [2, 3].

A. Sample selection from ATNF database

In the late times the number of pulsars has increased considerably [10]. Although various researchers have kept update catalogues, since then; in general, these have been neither completed nor very accessible. The ATNF database is an effort among an Australian scientific community and some foreign partner institutions. The purpose is to compile the largest amount of information about pulsars, which is subsequently made available to every researcher all over the world.

The ATNF catalogue [10] registers all published rotation-powered pulsars, including those detected only



(a)GW signals from pulsar acceleration and gamma-ray burst. Distribution (with the viewing angle) of the GW signal produced during the early acceleration phase of a pulsar (dashed–green line) with $V_{\star}^{\text{ave}} = 450 \text{ km s}^{-1}$, and distance = 10 kpc. Comparison with the GW signal from a gamma-ray burst (solid–red line), as a function of the jet angle to the line-of-sight, with parameters $\langle E \rangle = 10^{51} \text{ erg}$, $\gamma = 100$, and distance = 1 Mpc.

FIG. 2: Angular distribution of the GW signals from pulsar acceleration and gamma-ray burst

at high energies. It also records Anomalous X-ray Pulsars AXP and Soft Gamma-ray Repeaters (SGRs) for which coherent pulsations have been detected. However, it excludes accretion-powered pulsars such as Her X-1 and the recently discovered X-ray millisecond pulsars, for instance SAX J1808.4-3658 [15].

The ATNF catalogue [10] can be accessed in a number of different ways. The simplest one is from a web interface [28] allowing listing of the most commonly used pulsar parameters, together with the uncertainties and information on the references. Several options for *tabular output* format are provided. Currently, a total of 67 “predefined parameters” are available. A tool is provided for plotting of parameter distributions, either as two-dimensional plots or as histograms. Zoom tools and interactive identification of plotted points are provided. Custom parameters can be defined by combining parameters in expressions using mathematical operators and functions and these can be either listed or plotted. Finally, the sample of pulsars listed or plotted can be limited by logical conditions on parameters (see Table-I), pulsar name (including wild-card names) or distance from a nominated position. These operational tools are described in more detail below and links are provided within the web interface to relevant documentation [10].

In this particular case, we select from ATNF, by

clicking on the box to the left of the “parameter label” to select a couple of pulsar parameters: DIST and VTRANS (see Fig.1(c)). The first parameter is the best estimate of the pulsar distance in kpc. The second parameter is the transverse velocity, given in km s^{-1} , based on DIST estimates. By default the results will be sorted according to the pulsars’ J2000 names in ascending alphabetical order. However, sorting is possible on any parameter by typing the parameter label in the “sort on field text box” and selecting whether the sort should be in ascending (default) or descending order. However, to obtain as much information as possible some careful procedures must be followed. Because of this, we selected the listing fashion “short format without errors”. The short format is used to provide a condensed summary of the pulsars parameters (see Table-V). Finally, we selected the option “header”, that produces a table with header information at the top and selected the output option “Table” (see Table-I). Besides, it is possible to display functions of the pulsar parameters as a graph or as a histogram. For a normal (x-y) graph, the values to plot are defined as regular expressions into the “x, y-axis text box”, and the axes of the graph can be displayed linearly or logarithmically. The expressions may also contain custom-defined variables or externally defined variables.

III. PRESENT GALACTIC PULSAR DYNAMICS HINTS AT DETECTABILITY OF GW SIGNALS FROM THE SHORT RISE FLING OF RAPS IN SUPERNOVAE

Next we discuss the prospective for the short rise fling of Galactic RAPS in a supernova to generate detectable GW signals. The analysis starts from the observed kinematic state of RAPS, and goes back to their kicks at birth. To such an approach we assume that before the kick the star velocity is $V_{\star}^0 = 0$ [7].

First, let us notice that one can combine the first three pieces discussed above together with the extremely restrictive character of the thrust timescale ($\Delta T_{\text{max}}^{\text{kick}}$), the magnitude of the largest velocity (V_{\star}^{max}), and the instantaneous nature of the kick ($V_{\star}^0 = 0$). In so doing, one can then conclude that whichever the driving engine might be, it should transfer to the star at the kick at birth an energy as large as $\langle \Delta E \rangle \sim 10^{51} \text{ erg}$. (Recall that the NS masses are piled-up around $1.4 M_{\odot}$). Besides, keep in mind that according to Newton’s second law: $F_{\star} = M_{\star} a_{\star}$, the star’s inertia depends directly on its rest mass M_{\star} . Thus, putting together these ingredients one can conclude that the effective acceleration, a_{\star} , at the kick at birth of each RAP should be the same.[29] In other words, because pulsar velocities vary by more than an order of magnitude, whilst the inertia (mass) of each neutron star is essentially the same (within an uncertainty no greater than a factor of 2), one concludes that the acceleration at the kick at birth for each of the pulsars has definitely to be the same. In all our analysis

below we will use this key feature.

Further, as the kick is an “instantaneous action”, then the Newtonian kinematics states that the largest velocity[30] should be attained after the longest acceleration phase. That is; over the longest traction time t_*^{kick} . Therefore, the RAP kinematics during the short rise fling follows the law

$$V_*^{\text{fin}}(t) = V_*^0 + a_* \cdot t_*^{\text{kick}}, \quad (1)$$

where $V_*^{\text{fin}}(t)$ defines the final (at the end of the kick) velocity of a given RAP, which is reached after a total impulsion time t_*^{kick} . Consequently, if one assumes for the sake of simplicity that the RAP transit through the interstellar space does not modify its starting state of drifting, then one concludes that the largest (presently observed velocity $V_*^{\text{max}} \simeq 5000 \text{ km s}^{-1}$) must have been reached after the elapsing of the longest timescale permitted by the kick mechanism: $\Delta T_{\text{max}}^{\text{kick}} \simeq 0.32 \text{ s}$ [5].

Thus, after collecting all the pieces on the RAPs physics described above one can infer the characteristic acceleration received by a typical RAP. To this goal one can take the largest present velocity given by Refs. [2, 3, 4, 10] (see Fig.-1(c)), and the constraint on the maximum traction timescale for the kick at birth[5]. That acceleration then reads

$$a_* = \frac{V_*^{\text{max}}}{\Delta T_{\text{max}}^{\text{kick}}} \sim 10^4 \text{ km s}^{-2}. \quad (2)$$

A. Estimates of present h_c , f_{GW} GW characteristics hint at prospective detection during RAPs short rise fling in supernovae

The above analysis suggests that the overall time scale for acceleration of any given RAP to its present velocity (under the assumption stated above) depends exclusively on the total energy with which it was thrust. The actual amount of energy expended to thrust the star certainly has something to do with the nature of the driving mechanism. Hence, the GW dynamics to be discussed below, combined with observations of Galactic RAPs, may help to enlighten the path to unravel the actual thruster. Next we provide order of magnitude estimates for both GW amplitude and frequency based on parameters of RAPs currently cataloged. (In the next Section a rigorous derivation of these GW characteristics for the RAP kick at birth is presented).

1. Frequency estimate

From Eqs.(1)-(2) one can see that the traction time scale for any given pulsar is strictly directly proportional to its present spatial velocity. This is a conclusion of basic importance. That is, the RAP current kinematics

must retain information about what happened during its short rise fling in the supernova. Thus, the frequency of the GW burst emitted during the early impulsion of a pulsar in a supernova explosion can be assumed, in a very simplified picture, as being inversely related to the total acceleration time [18], that is,

$$f_{\text{GW}}^{\text{kick}} \simeq \frac{1}{t_*^{\text{kick}}}. \quad (3)$$

As an example, let us take the values quoted above for V_*^{max} , V_*^{ave} , and V_*^{min} . In these cases, one obtains the GW frequencies $f_{\text{GW}}^{\text{min}} = 3.1 \text{ Hz}$, $f_{\text{GW}}^{\text{ave}} = 34.7 \text{ Hz}$, and $f_{\text{GW}}^{\text{max}} = 186.0 \text{ Hz}$, respectively. It is illustrative to compare these frequencies with those provided in Figs.- (6, 7, 8, 9) below. As shown next, the last ones would be detectable by present-day laser-beam interferometers whenever their associate strains (computed below) are large enough (see Fig.3 for the estimates of h and f_{GW} for the 212 ATNF RAPs sample).

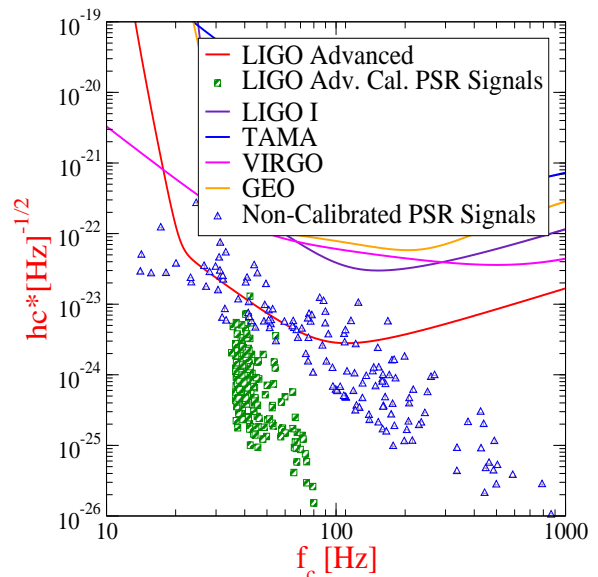


FIG. 3: *Color Online.* LIGO I, LIGO Advanced, VIRGO, GEO-600, TAMA-300 strain sensitivities and the h_c and f_c characteristics of the GW signal produced by each of the 212 pulsars calibrated with respect to LIGO Advanced (green squares), and the same sample without calibration (blue triangles). The effect of the calibration procedure is evident.

2. Amplitude estimate

To have an order of magnitude estimate of the GW amplitude, h , from the present kinematic state of a galactic RAP one can use the general relativistic quadrupole formula

$$h \simeq \frac{4G}{c^4} \frac{E_k}{r}, \quad (4)$$

where r is the pulsar distance as provided by the ATNF Catalog, and $E_k = \frac{1}{2}M_*V_*^2$ is the RAP kinetic energy.

Therefore, if one combines the theoretical prediction provided by Eq.(3) with this approximate GW amplitude, one obtains the plot presented in Fig.(3). The estimates were performed for a sample of 212 pulsars selected from the Australian Telescope National Facility (ATNF) catalog [1].[31] Notice that Eq.(4) states that whenever the RAP velocity is time-varying the signals, whose representative points appear above the strain sensitivity limit of Advanced LIGO, would be detectable by this observatory. For a RAP with no time-varying velocity, the signal would be a direct-current-like (DC) signal that no detector might observe. (Regarding the above estimates, keep in mind that at least the pulsar motion around the Galactic center (the bulge) should be

centripetally accelerated).

In Fig.-3 blue triangles represent GW signals computed following this back-of-the-envelope technique. Green squares are the obtained after calibrating the approximated signals against the strain sensitivity of Advanced LIGO. Clearly only a few RAPs would be detectable if their GW signals were described in such an approximate fashion. Moreover, this graph gives us a clear hint at the proper characteristics of the GW signal that would be emitted by a run away pulsar during its short rise fling in the supernova that makes it to drift across the galaxy. These order of magnitude estimates suggest that a RAP that was kicked out from the supernova ejecta with higher speed and acceleration would produce a clearly detectable GW signal. This perspective motivated us to study the problem using a more rigorous physical description: the theory for the emission of gravitational wave signals by ultrarelativistic sources, a GW signal which has memory. This is done in the next Section.

TABLE I: Full pulsar sample taken from ATNF. JName is the pulsar name based on J2000 coordinates, RAJ right ascension (J2000) in hh:mm:ss.s, DECJ declination (J2000) in +dd:mm:ss, PMRA proper motion in right ascension in mas yr⁻¹ units, PMDEC proper motion in declination in mas yr⁻¹ units, DIST best estimate of the pulsar distance in kpc units, VTRANS transverse velocity - based on DIST in km s⁻¹

#	PSR[J] Name	RAJ (hms)	DECJ (dms)	PMRA (mas/yr)	PMDEC (mas/yr)	DIST (kpc)	VTRANS (km/s)
1	J0014+4746	00:14:17.7	+47:46:33.4	19.300	-19.700	1.82	237.964
2	J0024-7204C	00:23:50.3	-72:04:31.4	5.200	-3.400	4.80	141.384
3	J0024-7204D	00:24:13.8	-72:04:43.8	3.800	-2.400	4.80	102.278
4	J0024-7204E	00:24:11.1	-72:05:20.1	6.200	-2.700	4.80	153.889
5	J0024-7204F	00:24:03.8	-72:04:42.8	4.600	-2.900	4.80	123.747
6	J0024-7204G	00:24:07.9	-72:04:39.6	4.200	-3.700	4.80	127.376
7	J0024-7204H	00:24:06.7	-72:04:06.7	5.100	-3.600	4.80	142.060
8	J0024-7204I	00:24:07.9	-72:04:39.6	4.900	-3.900	4.80	142.515
9	J0024-7204J	00:23:59.4	-72:03:58.7	5.350	-3.420	4.80	144.498
10	J0024-7204N	00:24:09.1	-72:04:28.8	6.800	-1.100	4.80	156.757
11	J0024-7204O	00:24:04.6	-72:04:53.7	4.600	-2.900	4.80	123.747
12	J0024-7204U	00:24:09.8	-72:03:59.6	5.100	-4.500	4.80	154.779
13	J0030+0451	00:30:27.4	+04:51:39.7	C	C	0.30	8.246
14	J0034-0534	00:34:21.8	-05:34:36.6	C	C	0.98	146.280
15	J0040+5716	00:40:32.3	+57:16:24.9	C	C	4.48	161.755
16	J0117+5914	01:17:38.6	+59:14:38.3	C	C	2.14	186.526
17	J0134-2937	01:34:18.6	-29:37:16.9	C	C	1.78	189.641
18	J0139+5814	01:39:19.7	+58:14:31.7	-21.000	-5.000	2.89	295.772
19	J0147+5922	01:47:44.6	+59:22:03.2	C	C	1.91	96.870
20	J0151-0635	01:51:22.7	-06:35:02.8	15.000	-30.000	1.93	306.902
21	J0152-1637	01:52:10.8	-16:37:52.9	3.100	-27.000	0.79	101.789
22	J0206-4028	02:06:01.2	-40:28:04.3	-10.000	75.000	0.88	315.673
23	J0218+4232	02:18:06.3	+42:32:17.4	C	C	5.85	138.673
24	J0255-5304	02:55:56.2	-53:04:21.3	0.000	70.000	1.15	381.648
25	J0304+1932	03:04:33.1	+19:32:51.4	6.000	-37.000	0.95	168.822
26	J0323+3944	03:23:26.6	+39:44:52.9	16.000	-30.000	1.49	240.177
27	J0332+5434	03:32:59.3	+54:34:43.5	17.000	-9.500	1.06	98.220
28	J0335+4555	03:35:16.6	+45:55:53.4	C	C	2.08	63.143
29	J0357+5236	03:57:44.8	+52:36:57.7	C	C	4.73	242.561
30	J0358+5413	03:58:53.7	+54:13:13.7	9.200	8.170	1.10	64.102
31	J0406+6138	04:06:30.0	+61:38:40.9	C	C	3.05	942.673
32	J0415+6954	04:15:55.6	+69:54:09.8	C	C	1.57	94.151

TABLE I: Full sample taken from ATNF Catalog.

#	PSR[J] Name	RAJ (hms)	DECJ (dms)	PMRA (mas/yr)	PMDEC (mas/yr)	DIST (kpc)	VTRANS (km/s)
33	J0437-4715	04:37:15.8	-47:15:08.8	121.310	-71.530	0.16	105.977
34	J0452-1759	04:52:34.0	-17:59:23.4	12.000	18.000	3.14	322.047
35	J0454+5543	04:54:07.7	+55:43:41.5	52.000	-17.000	0.79	204.903
36	J0502+4654	05:02:04.5	+46:54:06.0	-8.000	8.000	1.78	95.475
37	J0525+1115	05:25:56.4	+11:15:19.0	30.000	-4.000	7.68	1101.985
38	J0528+2200	05:28:52.3	+22:00:01	-20.000	7.000	2.28	229.047
39	J0534+2200	05:34:31.9	+22:00:52.0	-14.700	2.000	2.00	140.669
40	J0538+2817	05:38:25.0	+28:17:09.3	-23.530	52.590	1.47	401.682
41	J0543+2329	05:43:09.6	+23:29:05	19.000	12.000	3.54	377.151
42	J0601-0527	06:01:58.9	-05:27:50.5	18.000	-16.000	7.54	860.899
43	J0610-2100	06:10:13.5	-21:00:28.0	7.000	11.000	5.64	348.635
44	J0612+3721	06:12:48.6	+37:21:37.3	C	C	1.49	49.950
45	J0613-0200	06:13:43.9	-02:00:47.1	2.100	-10.500	0.48	24.174
46	J0614+2229	06:14:17.1	+22:30:36	-4.000	-3.000	4.74	112.361
47	J0621+1002	06:21:22.1	+10:02:38.7	3.500	-0.300	1.88	31.310
48	J0629+2415	06:29:05.7	+24:15:43.3	-7.000	2.000	4.67	161.184
49	J0630-2834	06:30:49.4	-28:34:43.1	-44.600	20.000	2.15	498.228
50	J0633+1746	06:33:54.1	+17:46:12.9	138.000	97.000	0.16	124.953
51	J0653+8051	06:53:15.0	+80:52:00.2	19.000	-1.000	3.37	303.984
52	J0659+1414	06:59:48.1	+14:14:21.5	44.070	-2.400	0.29	60.300
53	J0700+6418	07:00:37.8	+64:18:11.2	C	C	0.48	22.757
54	J0711-6830	07:11:54.2	-68:30:47.4	-11.000	19.000	1.04	108.249
55	J0737-3039A	07:37:51.2	-30:39:40.7	-3.300	2.600	0.33	6.639
56	J0737-3039B	07:37:51.2	-30:39:40.7	-3.300	2.600	0.33	6.639
57	J0738-4042	07:38:32.3	-40:42:40.9	-14.000	13.000	11.03	999.054
58	J0742-2822	07:42:49.0	-28:22:43.7	-29.000	4.000	1.89	262.313
59	J0751+1807	07:51:09.1	+18:07:38.6	C	C	0.62	17.809
60	J0754+3231	07:54:40.6	+32:31:56.2	-4.000	7.000	3.92	149.834
61	J0758-1528	07:58:29.0	-15:28:08.7	1.000	4.000	3.72	72.717
62	J0814+7429	08:14:59.5	+74:29:05.7	24.020	-44.000	0.43	102.883
63	J0820-1350	08:20:26.3	-13:50:55.4	9.000	-47.000	2.45	555.841
64	J0823+0159	08:23:09.7	+01:59:12.4	5.000	-1.000	1.44	34.811
65	J0826+2637	08:26:51.3	+26:37:23.7	61.000	-90.000	0.36	184.091
66	J0835-4510	08:35:20.6	-45:10:34.8	-49.680	29.900	0.29	78.542
67	J0837+0610	08:37:05.6	+06:10:14.5	2.000	51.000	0.72	174.222
68	J0837-4135	08:37:21.1	-41:35:14.3	-2.300	-18.000	4.24	364.772
69	J0846-3533	08:46:06.0	-35:33:40.7	93.000	-15.000	1.43	638.649
70	J0908-1739	09:08:38.1	-17:39:37.6	27.000	-40.000	0.63	144.143
71	J0922+0638	09:22:14.0	+06:38:23.3	18.800	86.400	1.20	505.062
72	J0943+1631	09:43:30.1	+16:31:37	23.000	9.000	1.76	206.084
73	J0944-1354	09:44:28.9	-13:54:41.6	-1.000	-22.000	0.69	72.042
74	J0946+0951	09:46:07.6	+09:51:55	-38.000	-21.000	0.98	201.720
75	J0953+0755	09:53:09.3	+07:55:35.7	-2.090	29.460	0.26	36.654
76	J1012+5307	10:12:33.4	+53:07:02.5	2.400	-25.200	0.52	62.407
77	J1024-0719	10:24:38.6	-07:19:19.1	-34.900	-47.000	0.53	146.072
78	J1041-1942	10:41:36.1	-19:42:13.6	-1.000	14.000	3.18	211.606
79	J1045-4509	10:45:50.1	-45:09:54.1	-7.000	8.000	3.24	163.287
80	J1115+5030	11:15:38.4	+50:30:12.2	22.000	-51.000	0.54	142.196
81	J1116-4122	11:16:43.0	-41:22:43.9	-1.000	7.000	2.68	89.843
82	J1136+1551	11:36:03.2	+15:51:04.4	-74.000	368.100	0.36	635.733
83	J1239+2453	12:39:40.4	+24:53:49.2	-104.500	49.400	0.86	472.410
84	J1300+1240	13:00:03.0	+12:40:56.7	46.400	-82.200	0.77	344.234
85	J1321+8323	13:21:46.1	+83:23:38.9	-53.000	13.000	0.77	199.214
86	J1328-4357	13:28:06.4	-43:57:44.1	3.000	54.000	2.29	587.172
87	J1430-6623	14:30:40.8	-66:23:05.0	-31.000	-21.000	1.80	319.531
88	J1453-6413	14:53:32.7	-64:13:15.5	-16.000	-21.300	1.84	232.391
89	J1455-3330	14:55:47.9	-33:30:46.3	5.000	24.000	0.74	86.007
90	J1456-6843	14:56:00.1	-68:43:39.2	-39.500	-12.300	0.45	89.153
91	J1509+5531	15:09:25.6	+55:31:32.3	-73.606	-62.622	2.41	1104.013

TABLE I: Full sample taken from ATNF Catalog.

#	PSR[J] Name	RAJ (hms)	DECJ (dms)	PMRA (mas/yr)	PMDEC (mas/yr)	DIST (kpc)	VTRANS (km/s)
92	J1518+4904	15:18:16.7	+49:04:34.2	C	C	0.70	30.914
93	J1537+1155	15:37:09.9	+11:55:55.5	1.340	-25.050	0.90	107.038
94	J1543-0620	15:43:30.1	-06:20:45.2	-17.000	-4.000	1.15	95.217
95	J1543+0929	15:43:38.8	+09:29:16.5	-7.300	-4.000	2.46	97.082
96	J1559-4438	15:59:41.5	-44:38:46.1	1.000	14.000	1.58	105.137
97	J1600-3053	16:00:51.9	-30:53:49.3	-1.020	-6.700	2.67	85.788
98	J1603-7202	16:03:35.6	-72:02:32.6	-2.800	-6.000	1.64	51.481
99	J1604-4909	16:04:22.9	-49:09:58.3	-30.000	-1.000	3.59	510.886
100	J1607-0032	16:07:12.1	+00:32:40.8	-1.000	-7.000	0.59	19.779
101	J1623-2631	16:23:38.2	-26:31:53.7	-13.400	-25.000	2.20	295.848
102	J1640+2224	16:40:16.7	+22:24:08.9	1.660	-11.300	1.19	64.436
103	J1643-1224	16:43:38.1	-12:24:58.7	3.000	-8.000	4.86	196.863
104	J1645-0317	16:45:02.0	-03:17:58.3	-3.700	30.000	2.91	417.022
105	J1709-1640	17:09:26.4	-16:40:57.7	3.000	0.000	1.27	18.063
106	J1709+2313	17:09:05.7	+23:13:27.8	-3.200	-9.700	1.83	88.618
107	J1713+0747	17:13:49.5	+07:47:37.5	4.917	-3.933	1.12	33.541
108	J1720-0212	17:20:57.2	-02:12:23.9	-1.000	-26.000	5.41	667.357
109	J1722-3207	17:22:02.9	-32:07:45.3	-1.000	-40.000	3.18	603.239
110	J1735-0724	17:35:04.9	-07:24:52.4	-2.400	28.000	4.32	575.570
111	J1738+0333	17:38:53.9	+03:33:10.8	5.600	4.000	1.97	64.275
112	J1740+1311	17:40:07.3	+13:11:56.6	-22.000	-20.000	4.77	672.375
113	J1741-3927	17:41:18.0	-39:27:38.0	20.000	-6.000	4.75	470.223
114	J1744-1134	17:44:29.4	-11:34:54.6	19.600	-7.000	0.48	46.986
115	J1745-3040	17:45:56.3	-30:40:23.5	6.000	4.000	2.08	71.110
116	J1752-2806	17:52:58.6	-28:06:37.3	-4.000	-5.000	1.53	46.446
117	J1801-2451	18:00:59.8	-24:51:53	2.000	-3.000	4.61	78.802
118	J1801-1417	18:01:51.0	-14:17:34.5	-8.000	-23.000	1.80	207.810
119	J1803-2137	18:03:51.4	-21:37:07.3	11.600	14.800	3.94	351.252
120	J1807-0847	18:07:38.0	-08:47:43.2	-5.000	1.000	3.60	87.027
121	J1820-0427	18:20:52.6	-04:27:38.1	C	C	2.45	164.266
122	J1823+0550	18:23:30.9	+05:50:24.3	5.000	-2.000	3.01	76.848
123	J1824-1945	18:24:00.4	-19:45:51.7	-12.000	-100.000	5.20	2482.989
124	J1824-2452	18:24:32.0	-24:52:11.1	-0.900	-4.600	4.90	108.887
125	J1825-0935	18:25:30.5	-09:35:22.1	-13.000	-9.000	1.00	74.961
126	J1829-1751	18:29:43.1	-17:51:03.9	22.000	-150.000	5.49	3945.954
127	J1832-0827	18:32:37.0	-08:27:03.6	-4.000	20.000	4.75	459.311
128	J1833-0827	18:33:40.3	-08:27:31.2	C	C	5.67	901.625
129	J1835-1106	18:35:18.2	-11:06:15.1	27.000	56.000	3.08	907.804
130	J1836-0436	18:36:51.7	-04:36:37.6	C	C	4.62	265.780
131	J1836-1008	18:36:53.9	-10:08:08.3	18.000	12.000	5.39	552.813
132	J1840+5640	18:40:44.6	+56:40:55.4	-30.000	-21.000	1.70	295.141
133	J1841-0425	18:41:05.6	-04:25:19.6	C	C	5.17	285.843
134	J1844+1454	18:44:54.8	+14:54:14.1	-9.000	45.000	2.23	485.178
135	J1850+1335	18:50:35.4	+13:35:58.3	C	C	3.14	240.040
136	J1857+0943	18:57:36.3	+09:43:17.2	-2.940	-5.410	0.91	26.537
137	J1900-2600	19:00:47.5	-26:00:43.8	-19.900	-47.300	2.00	486.568
138	J1902+0615	19:02:50.2	+06:16:33.4	C	C	9.63	368.086
139	J1905-0056	19:05:27.7	-00:56:40.9	C	C	6.91	296.655
140	J1906+0641	19:06:35.2	+06:41:02.9	C	C	9.23	269.607
141	J1907+4002	19:07:34.6	+40:02:05.7	11.000	11.000	1.76	129.804
142	J1909+1102	19:09:48.6	+11:02:03.3	C	C	4.31	192.770
143	J1909-3744	19:09:47.4	-37:44:14.3	-9.490	-36.060	1.14	200.885
144	J1910-5959A	19:11:42.7	-59:58:26.9	-3.300	-3.600	4.00	92.613
145	J1910-5959C	19:11:05.5	-60:00:59.7	-4.100	-4.600	4.00	116.855
146	J1911-1114	19:11:49.2	-11:14:22.3	-6.000	-23.000	1.59	179.179
147	J1913+1400	19:13:24.3	+14:00:52.7	C	C	5.07	326.934
148	J1913-0440	19:13:54.1	-04:40:47.6	7.000	-5.000	3.22	131.322
149	J1915+1009	19:15:29.9	+10:09:43.7	C	C	5.32	177.003
150	J1915+1606	19:15:27.9	+16:06:27.4	-2.560	0.490	7.13	88.107

TABLE I: Full sample taken from ATNF Catalog.

#	PSR[J] Name	RAJ (hms)	DECJ (dms)	PMRA (mas/yr)	PMDEC (mas/yr)	DIST (kpc)	VTRANS (km/s)
151	J1916+0951	19:16:32.3	+09:51:25.9	C	C	2.88	123.257
152	J1917+1353	19:17:39.7	+13:53:56.9	0.000	-6.000	4.07	115.774
153	J1919+0021	19:19:50.6	+00:21:39.8	-2.000	-1.000	3.32	35.196
154	J1921+2153	19:21:44.8	+21:53:02.2	17.000	32.000	0.66	113.382
155	J1926+1648	19:26:45.3	+16:48:32.7	C	C	7.74	597.353
156	J1932+1059	19:32:13.9	+10:59:32.4	94.090	42.990	0.36	177.051
157	J1935+1616	19:35:47.8	+16:16:40.2	-1.000	-13.000	7.93	490.190
158	J1937+2544	19:37:01.2	+25:44:13.6	C	C	2.76	232.973
159	J1939+2134	19:39:38.5	+21:34:59.1	-0.460	-0.660	3.60	13.731
160	J1941-2602	19:41:00.4	-26:02:05.7	12.000	-10.000	4.74	351.027
161	J1944+0907	19:44:09.3	+09:07:23.2	12.000	-18.000	1.28	131.280
162	J1946-2913	19:46:51.7	-29:13:47.1	19.000	-33.000	4.31	778.087
163	J1946+1805	19:46:53.0	+18:05:41.2	1.000	-9.000	0.85	36.492
164	J1948+3540	19:48:25.0	+35:40:11.0	-12.600	0.700	7.87	470.849
165	J1952+3252	19:52:58.2	+32:52:40.5	-24.000	-8.000	2.50	299.845
166	J1954+2923	19:54:22.5	+29:23:17.2	25.000	-36.000	0.42	87.273
167	J1955+2908	19:55:27.8	+29:08:43.5	-1.000	-3.700	5.39	97.941
168	J1955+5059	19:55:18.7	+50:59:55.2	-23.000	54.000	1.80	500.880
169	J1959+2048	19:59:36.7	+20:48:15.1	-16.000	-25.800	1.53	220.211
170	J2002+4050	20:02:44.0	+40:50:53.9	C	C	8.30	524.995
171	J2004+3137	20:04:52.2	+31:37:10.0	C	C	8.94	473.870
172	J2013+3845	20:13:10.3	+38:45:43.3	-32.100	-25.000	13.07	2521.130
173	J2018+2839	20:18:03.8	+28:39:54.2	-2.600	-6.200	0.97	30.945
174	J2019+2425	20:19:31.9	+24:25:15.3	-9.410	-20.600	0.91	97.708
175	J2022+2854	20:22:37.0	+28:54:23.1	-4.400	-23.600	2.70	307.605
176	J2022+5154	20:22:49.8	+51:54:50.2	-5.230	11.500	2.00	119.788
177	J2023+5037	20:23:41.9	+50:37:34.8	C	C	1.80	187.936
178	J2046-0421	20:46:00.1	-04:21:26.0	9.000	-7.000	3.83	207.032
179	J2046+1540	20:46:39.3	+15:40:33.6	-13.000	3.000	2.56	161.926
180	J2048-1616	20:48:35.4	-16:16:43.0	117.000	-5.000	0.64	355.328
181	J2051-0827	20:51:07.5	-08:27:37.7	5.300	0.300	1.28	32.214
182	J2055+2209	20:55:39.1	+22:09:27.2	C	C	2.15	52.413
183	J2055+3630	20:55:31.3	+36:30:21.4	-3.000	3.000	5.56	111.835
184	J2108+4441	21:08:20.4	+44:41:48.8	3.500	1.400	5.28	94.362
185	J2113+2754	21:13:04.3	+27:54:02.2	-23.000	-54.000	1.39	386.791
186	J2113+4644	21:13:24.3	+46:44:08.7	C	C	4.99	308.455
187	J2116+1414	21:16:13.7	+14:14:21.0	8.000	-11.000	4.43	285.665
188	J2124-3358	21:24:43.8	-33:58:44.6	-14.400	-50.000	0.25	61.670
189	J2129+1210A	21:29:58.2	+12:10:01.2	-0.260	-4.400	8.90	185.980
190	J2129+1210B	21:29:58.6	+12:10:00.3	1.700	-1.900	8.90	107.576
191	J2129+1210C	21:30:01.2	+12:10:38.2	-1.300	-3.300	10.00	168.154
192	J2129-5721	21:29:22.7	-57:21:14.1	7.000	-4.000	2.55	97.468
193	J2145-0750	21:45:50.4	-07:50:18.3	C	C	0.50	33.461
194	J2149+6329	21:49:58.5	+63:29:43.5	14.000	10.000	13.65	1113.385
195	J2150+5247	21:50:37.7	+52:47:49.6	C	C	5.67	231.241
196	J2157+4017	21:57:01.8	+40:17:45.8	17.800	2.800	5.58	476.682
197	J2219+4754	22:19:48.1	+47:54:53.9	-12.000	-30.000	2.45	375.304
198	J2225+6535	22:25:52.4	+65:35:34.0	144.000	112.000	2.00	1729.770
199	J2229+6205	22:29:41.8	+62:05:36.0	C	C	5.70	270.235
200	J2229+2643	22:29:50.8	+26:43:57.7	1.000	-17.000	1.43	115.452
201	J2235+1506	22:35:43.7	+15:06:49.0	15.000	10.000	1.15	98.289
202	J2257+5909	22:57:57.7	+59:09:14.8	C	C	6.40	540.227
203	J2257+5909	22:57:57.7	+59:09:14.8	C	C	6.40	540.227
204	J2305+3100	23:05:58.3	+31:00:01.7	2.000	-20.000	3.92	373.546
205	J2308+5547	23:08:13.8	+55:47:36.0	-15.000	0.000	2.42	172.097
206	J2313+4253	23:13:08.5	+42:53:12.9	C	C	0.95	99.296
207	J2317+1439	23:17:09.2	+14:39:31.2	-1.700	7.400	1.89	68.034
208	J2321+6024	23:21:55.2	+60:24:30.7	-17.000	-7.000	3.21	279.789
209	J2322+2057	23:22:22.3	+20:57:02.9	-17.000	-18.000	0.78	91.557

TABLE I: Full sample taken from ATNF Catalog.

#	PSR[J] Name	RAJ (hms)	DECJ (dms)	PMRA (mas/yr)	PMDEC (mas/yr)	DIST (kpc)	VTRANS (km/s)
210	J2326+6113	23:26:58.6	+61:13:36.4	C	C	4.82	433.576
211	J2330-2005	23:30:26.8	-20:05:29.6	74.700	5.000	0.49	173.922
212	J2337+6151	23:37:05.7	+61:51:01.6	C	C	2.47	124.481
213	J2354+6155	23:54:04.7	+61:55:46.7	22.000	6.000	3.31	357.846

From the analysis of this Table one can realize that most of the SNR that were obtained gather about an $S/N \sim \mathcal{O}(1)$. However, an SNR of the order of unity is not enough for detection. The statistics which is the output of the *matched filter* must stand over the GW detector noise. Thus, if one assumes Gaussian noise in the detector and a Gaussian distributed statistics, then an SNR of something like 5, *what means a chance of one in a million*, is required to state that *it is signal and not noise*. Notwithstanding, RAPs current kinematics suggest that the dynamical situation could have been dramatically different during the short rise fling that launches each pulsar to drift across the Galaxy. In virtue of the potentiality of this phenomenon for the emission of powerful gravitational radiation signals, in the next Section we analyze the pulsar kick at birth within the framework of a theory that appears more appropriate to describe that process, and reestimate the characteristics of the GW released.

IV. GRAVITATIONAL WAVES FROM PULSAR ACCELERATION

Observations of extragalactic astrophysical sources suggest that blobs of matter are ejected with ultrarelativistic speeds (Lorentz factor $\gamma \gg 1$) in various powerful phenomena involving quasars, active galactic nuclei, radio-galaxies, supernova explosions, and microquasars. For these sources the emission of gravitational waves when such an ultrarelativistic blob is ejected from the core of its host source have been studied by Segalis and Ori[19] (see also [18] for the analysis of similar phenomena in gamma-ray bursts).

Supernova explosions are known to be the natural place of birth of neutron stars and pulsars, e. g. *The Crab Nebula*. In processes such these, the nascent pulsar is kicked out from the supernova remnant with speed that is not so large as compared to that for the blobs in AGN or quasars, where a significant fraction of the speed of light is typical for the ejecta. Nonetheless, the velocity at birth can be considered large if one bears in mind that the typical mass of neutron stars is about one solar mass[8]. Although a galactic RAP cannot be considered an ultrarelativistic source, the pulsar rise fling during the supernova can kick it out with very high speed. That is why in the discussion below we analyze the gravitational radiation emitted during the kick at birth of RAPs within the framework of Ref.[19]. Besides, it is also of worth

to keep in mind that such an approach can be applied to the early RAPs dynamics because in this case the limit $\gamma \sim 1$ applies. This limit corresponds to the GW strain h provided by the well-known general relativistic quadrupole formula for the same dynamical situation [6]. But bear in mind that this does not describe properly the GW angular distribution.

The pulsar is envisioned hereafter as a “particle” of mass M_\star moving along the worldline $r^\lambda(\tau)$ (with τ the proper time) and having an energy-stress tensor

$$T_{\mu\nu}(x) = M_\star \int V_\mu V_\nu \delta^{(4)}[x - r(\tau)] d\tau, \quad (5)$$

where $V^\alpha = dr^\alpha/d\tau$ is the particle 4-vector velocity. (Upper[sub])scripts are raised[lowered] with the Minkowski metric $\eta_{\mu\nu}$).

Since we are using the linearized Einstein’s equations to describe the emission of GW during the early acceleration phase of any pulsar, then the resulting metric perturbation produced by the RAP can straightforwardly be evaluated at the retarded time, which corresponds to the intersection time of $r^\alpha(\tau)$ with the observer’s past light-cone, and then be transformed to the Lorentz gauge where it reads: $h_{\mu\nu} = \bar{h}_{\mu\nu} - \frac{1}{2}\eta_{\mu\nu}\bar{h}^\alpha_\alpha$. This strain can equivalently be written as

$$h_{\mu\nu} = \frac{4 M_\star}{-V_\lambda \cdot [x - r(\tau)]^\lambda} \left(V_\mu(\tau)V_\nu(\tau) + \frac{1}{2}\eta_{\mu\nu} \right). \quad (6)$$

Notice that is this factor $-V_\lambda \cdot [x - r(\tau)]^\lambda$; which depends on the velocity in the denominator of Eq.(6), that is responsible for the nonvanishing amplitude (GW “memory” [6]) of the GW signal produced by the launching of the pulsar into its present trajectory.

Eq.(6) must be finally rewritten in the transverse-traceless (*TT*) gauge, i. e. $h_{\mu\nu} \rightarrow h_{\mu\nu}^{TT}$; which is the best suited to discuss the GW detector’s response to that signal. This procedure leads to the result presented in Eq.(7).

A detailed analysis (see Refs.[6, 19]) shows that the maximum GW strain in the detector is obtained for a wavevector, \vec{n} , orthogonal to the detector’s arm, in the $\vec{v} - \vec{n}$ plane. Here \vec{n} is the unit spatial direction vector from the (retarded) pulsar position to the observer, and \vec{v} the unit spatial direction vector defining the 3-D pulsar velocity \vec{V} . In this case, the GW amplitude generated by the pulsar kick becomes (c.g.s. units recovered)

$$h_{\max}(t) = \left[\frac{G}{c^2} \right] \int_0^{\theta_V} 2 \frac{\gamma(t) M_{\star} \beta^2(t)}{D_{\star}} \left(\frac{\sin^3 \theta \sin 2\Delta\phi}{\Delta\Omega(1 - \beta \cos \theta)} \right) d\theta, \quad (7)$$

where θ is the angle between \vec{v} and \vec{n} , that is the angle between the unit spatial direction vector associated to the velocity of the pulsar, \vec{V} , and the unit spatial direction vector linking the source point to the observer location, i. e. $\vec{v} \cdot \vec{n} = \cos \theta$. θ_V is the particular (e. g. *Vela Pulsar*) viewing angle that a RAP velocity makes with the direction \vec{n} to the observer. $\Delta\theta$ is the angular diameter of the pulsar as seen by the observer. (For galactic distances it can be assumed nearly constant for each of the RAPs in the sample under analysis). Thus $\Delta\Omega \simeq \pi(\Delta\theta)^2$ is the solid angle over which the RAP is viewed. Besides, $\beta = |\vec{V}|/c$, being $|\vec{V}|$ the pulsar 3-D velocity $V_{\star}^{\text{fin}}(t)$ defined above, and γ the Lorentz factor; which can be taken here as ~ 1 because $V_{\star}^{\text{fin}}(t) \ll c$. It is also defined $\Delta\phi = \cos^{-1} \left(\frac{\cos \Delta\theta - \cos \theta_V \cos \theta}{\sin \theta_V \sin \theta} \right)$. Finally, the distance to the pulsar is D_{\star} .

This formula was obtained in the form presented above first by Sago et al.[18] in discussing the GW emission from gamma-ray bursts (GRBs). It is essentially equivalent to the formula obtained by Segalis and Ori [19] in an earlier paper in which they discussed the GW emission by ultrarelativistic sources. The main difference in between is related to the detailed description of the angular distribution of the gravitational radiation emitted in each of the cases that those authors analyzed. The formula indicates that the GW strain depends on the Lorentz factor, pulsar speed and distance to the observer, and also on the strong beaming effect in the case of GRBs, as indicated by the factors $(1 - \cos \theta)$, and $\Delta\Omega$, appearing in the denominator of the equation. These effects are no so much important in the case of Galactic RAPs, as is evident from the pulsar speed and angular size.

This result, shown in Fig.2, states that the GW space-time perturbation is not strongly beamed in the forward direction \vec{n} , as opposed to the case of the electromagnetic radiation in gamma-ray bursts (also shown in the same Figure). Instead, the metric perturbation at the ultra-relativistic limit (not applicable to RAPs) has a directional dependence scaling as $1 + \cos \theta$. In such a case, because of the strong beaming effect, as in gamma-ray bursts; for instance, the electromagnetic radiation emitted by the source over the same time interval is visible only inside the very small solid angle ($\theta \sim \gamma^{-1}$)², whereas the GW signal is observable within a wider solid angle; almost 2π radians (see Fig.2). Besides, the observed GW frequency is Doppler blueshifted in the forward direction, and therefore the energy flux carried by the GWs is beamed in the forward direction, too. Quite noticeable, in the case of RAPs the GW signal will have its maximum for viewing angles $\theta \sim \pi/2$, that is; for pulsar motions purely in the plane of the sky, as shown in Fig. 2. This key physical property of the emission process

allows us to neglect the radial component of the pulsar velocity because it does not contribute to the effective GW amplitude of the signal being emitted by the RAP, or in other words, to the signal to be detected on Earth.

TABLE II: Characteristic amplitude and frequency, h_c , f_c (Hz), and $S/N = h_c(f_c)/h_{rms}(f_c)$.

Jname	f_c	h_c	S/N
\hat{A}	[Hz]	\hat{A}	\hat{A}
J0014+4746	37.1239	7.99071×10^{-24}	0.465967
J0024-7204C	39.0641	1.81774×10^{-24}	0.114416
J0024-7204D	43.0236	1.13491×10^{-24}	0.0810649
J0024-7204E	38.1603	2.03054×10^{-24}	0.123401
J0024-7204F	40.5101	1.50882×10^{-24}	0.100293
J0024-7204G	40.1852	1.57348×10^{-24}	0.103335
J0024-7204H	39.0137	1.82934×10^{-24}	0.114923
J0024-7204I	38.98	1.83713×10^{-24}	0.115263
J0024-7204J	38.8167	1.87205×10^{-24}	0.116717
J0024-7204N	37.9712	2.07818×10^{-24}	0.125358
J0024-7204O	40.5101	1.50882×10^{-24}	0.100293
J0024-7204U	38.1007	2.04539×10^{-24}	0.124012
J0030+0451	79.288	2.32394×10^{-25}	0.0165996
J0034-0534	38.6853	9.31883×10^{-24}	0.578055
J0040+5716	37.6624	2.31387×10^{-24}	0.137876
J0117+5914	36.6742	5.64571×10^{-24}	0.323257
J0134-2937	36.5873	6.90089×10^{-24}	0.393722
J0139+5814	38.4259	5.93842×10^{-24}	0.364667
J0147+5922	43.9134	2.67217×10^{-24}	0.19087
J0151-0635	38.4397	9.25843×10^{-24}	0.568847
J0152-1637	43.0987	6.85662×10^{-24}	0.489759
J0206-4028	38.5556	2.08228×10^{-23}	1.28516
J0218+4232	39.2696	1.45314×10^{-24}	0.0921892
J0255-5304	39.0962	1.86966×10^{-23}	1.1783
J0304+1932	37.2766	1.14724×10^{-23}	0.673126
J0323+3944	37.1671	9.82703×10^{-24}	0.57405
J0332+5434	43.6786	4.89642×10^{-24}	0.349744
J0335+4555	53.156	1.38012×10^{-24}	0.09858
J0357+5236	37.143	3.12732×10^{-24}	0.182506
J0358+5413	52.7994	2.66806×10^{-24}	0.190576
J0406+6138	41.529	1.51989×10^{-23}	1.04865
J0415+6954	44.4139	3.13942×10^{-24}	0.224244
J0437-4715	42.4872	3.55097×10^{-23}	2.53527
J0452-1759	38.6709	5.93204×10^{-24}	0.367763
J0454+5543	36.4967	1.65967×10^{-23}	0.943389
J0502+4654	44.1655	2.817×10^{-24}	0.201214
J0525+1115	40.4211	7.49499×10^{-24}	0.496559
J0528+2200	36.9714	6.20109×10^{-24}	0.359381
J0534+2200	39.1178	4.33307×10^{-24}	0.273303
J0538+2817	39.3889	1.50976×10^{-23}	0.962179
J0543+2329	39.151	6.00026×10^{-24}	0.378942
J0601-0527	42.5181	5.41622×10^{-24}	0.386873
J0610-2100	38.8927	3.54204×10^{-24}	0.221485
J0612+3721	58.5628	1.34323×10^{-24}	0.0959447
J0613-0200	71.1509	1.16838×10^{-24}	0.0834554
J0614+2229	41.9176	1.30377×10^{-24}	0.091219
J0621+1002	67.466	4.79347×10^{-25}	0.0342391
J0629+2415	37.6964	2.21027×10^{-24}	0.131882
J0630-2834	40.8252	1.17533×10^{-23}	0.790392
J0633+1746	40.4001	4.59112×10^{-23}	3.03935
J0653+8051	38.4132	5.25441×10^{-24}	0.322503

TABLE II: results of full calculation of h_c , f_c and S/N .

Jname	f_c	h_c	S/N
\AA	[Hz]	\AA	\AA
J0659+1414	54.243	9.24396×10^{-24}	0.660283
J0700+6418	71.8931	1.04344×10^{-24}	0.0745312
J0711-6830	42.4243	5.59481×10^{-24}	0.398562
J0737-3039A	80.003	1.37444×10^{-25}	0.00981745
J0737-3039B	80.003	1.37444×10^{-25}	0.00981745
J0738-4042	41.1211	4.55418×10^{-24}	0.309597
J0742-2822	37.6139	8.28784×10^{-24}	0.492893
J0751+1807	74.4793	5.07004×10^{-25}	0.0362146
J0754+3231	38.44	2.40285×10^{-24}	0.147635
J0758-1528	49.8372	9.44338×10^{-25}	0.0674527
J0814+7429	42.932	1.27573×10^{-23}	0.911233
J0820-1350	41.3826	1.12452×10^{-23}	0.77176
J0823+0159	65.7034	7.55761×10^{-25}	0.0539829
J0826+2637	36.7006	3.31806×10^{-23}	1.90188
J0835-4510	48.0888	1.34572×10^{-23}	0.961228
J0837+0610	37.0345	1.56722×10^{-23}	0.910601
J0837-4135	39.0797	4.87755×10^{-24}	0.307197
J0846-3533	42.1711	2.1265×10^{-23}	1.50133
J0908-1739	38.8431	1.42168×10^{-23}	0.887279
J0922+0638	40.8917	2.12817×10^{-23}	1.43466
J0943+1631	36.5052	7.482×10^{-24}	0.425441
J0944-1354	50.0532	5.0256×10^{-24}	0.358971
J0946+0951	36.5382	1.31884×10^{-23}	0.750931
J0953+0755	64.7903	4.58178×10^{-24}	0.32727
J1012+5307	53.4332	5.4258×10^{-24}	0.387557
J1024-0719	38.7005	1.71988×10^{-23}	1.06749
J1041-1942	36.6277	4.21129×10^{-24}	0.240668
J1045-4509	37.5731	3.23577×10^{-24}	0.192124
J1115+5030	39.0036	1.62815×10^{-23}	1.02244
J1116-4122	45.2874	1.73472×10^{-24}	0.123909
J1136+1551	42.1747	8.4083×10^{-23}	5.9371
J1239+2453	40.3084	2.84975×10^{-23}	1.88014
J1300+1240	35.5643	2.88182×10^{-23}	1.57571
J1321+8323	36.5293	1.66243×10^{-23}	0.946228
J1328-4357	41.7366	1.25324×10^{-23}	0.871163
J1430-6623	38.6252	1.02823×10^{-23}	0.636333
J1453-6413	37.0066	7.7727×10^{-24}	0.451106
J1455-3330	46.1529	5.94254×10^{-24}	0.424467
J1456-6843	45.4369	1.0231×10^{-23}	0.730788
J1509+5531	40.5816	2.3723×10^{-23}	1.58107
J1518+4904	67.6675	1.25824×10^{-24}	0.0898742
J2127+1155	42.3434	6.41853×10^{-24}	0.455935
J1543-0620	44.2132	4.34578×10^{-24}	0.310413
J1543+0929	43.8759	2.08026×10^{-24}	0.14859
J1559-4438	42.6042	3.56121×10^{-24}	0.254372
J1600-3053	46.2049	1.64159×10^{-24}	0.117257
J1603-7202	57.8922	1.28057×10^{-24}	0.0914696
J1604-4909	40.8763	7.19655×10^{-24}	0.484865
J1607-0032	73.4576	6.51078×10^{-25}	0.0465056
J1623-2631	38.4278	7.80249×10^{-24}	0.479169
J1640+2224	52.6765	2.48508×10^{-24}	0.177506
J1643-1224	36.5278	2.60936×10^{-24}	0.148511
J1645-0317	39.5595	7.80952×10^{-24}	0.500944
J1709-1640	74.3462	2.54331×10^{-25}	0.0181665
J1709+2313	45.5546	2.4967×10^{-24}	0.178335
J1713+0747	66.3388	9.09886×10^{-25}	0.0649919
J1720-0212	41.9078	5.9315×10^{-24}	0.414854

TABLE II: results of full calculation of h_c , f_c and S/N .

Jname	f_c	h_c	S/N
\AA	[Hz]	\AA	\AA
J1722-3207	41.6931	9.28191×10^{-24}	0.644202
J1735-0724	41.8263	6.49042×10^{-24}	0.452622
J1738+0333	52.7357	1.49566×10^{-24}	0.106833
J1740+1311	42.0383	6.73415×10^{-24}	0.473193
J1741-3927	40.304	5.13915×10^{-24}	0.339001
J1744-1134	59.8904	3.77654×10^{-24}	0.269753
J1745-3040	50.3561	1.63708×10^{-24}	0.116934
J1752-2806	60.1363	1.16259×10^{-24}	0.0830422
J1801-2451	48.0157	8.50308×10^{-25}	0.0607363
J1801-1417	36.5256	7.3598×10^{-24}	0.418842
J1803-2137	38.877	5.109×10^{-24}	0.319274
J1807-0847	45.9144	1.24016×10^{-24}	0.0885829
J1820-0427	37.5413	4.30552×10^{-24}	0.255316
J1823+0550	48.5757	1.25897×10^{-24}	0.0899267
J1824-1945	40.9223	2.43213×10^{-23}	1.6414
J1824-2452	42.3423	1.19895×10^{-24}	0.085163
J1825-0935	49.139	3.6633×10^{-24}	0.261664
J1829-1751	54.6043	2.63599×10^{-23}	1.88285
J1832-0827	40.1473	5.06412×10^{-24}	0.332107
J1833-0827	41.7718	7.73006×10^{-24}	0.538018
J1835-1106	41.7953	1.43077×10^{-23}	0.996669
J1836-0436	37.6347	3.43269×10^{-24}	0.204318
J1836-1008	41.3733	5.08732×10^{-24}	0.349026
J1840+5640	38.4105	1.00787×10^{-23}	0.61854
J1841-0425	38.	3.26129×10^{-24}	0.196949
J1844+1454	40.4852	1.11881×10^{-23}	0.743005
J1850+1335	37.1645	4.66117×10^{-24}	0.272255
J1857+0943	69.9194	7.32693×10^{-25}	0.0523352
J1900-2600	40.5195	1.24926×10^{-23}	0.830687
J1902+0615	39.1075	2.16284×10^{-24}	0.136365
J1905-0056	38.4463	2.48948×10^{-24}	0.152996
J1906+0641	37.6858	1.73977×10^{-24}	0.103764
J1907+4002	39.9779	4.40831×10^{-24}	0.28727
J1909+1102	36.5478	2.89161×10^{-24}	0.16471
J1909-3744	36.5355	1.1301×10^{-23}	0.643394
J1910-5959A	44.7141	1.20734×10^{-24}	0.0862383
J1910-5959C	41.4165	1.64278×10^{-24}	0.112883
J1911-1114	36.8491	7.30991×10^{-24}	0.421542
J1913+1400	38.7526	3.7195×10^{-24}	0.231327
J1913-0440	39.8321	2.4511×10^{-24}	0.158855
J1915+1009	36.9264	2.15708×10^{-24}	0.124784
J1915+1606	45.6686	6.36111×10^{-25}	0.0454365
J1916+0951	40.7829	2.47226×10^{-24}	0.165997
J1917+1353	41.5323	1.59151×10^{-24}	0.109819
J1919+0021	65.5118	3.34207×10^{-25}	0.0238719
J1921+2212	41.7992	9.49871×10^{-24}	0.661766
J1926+1648	57.7089	3.11667×10^{-24}	0.222619
J1932+1059	36.9246	3.18859×10^{-23}	1.84443
J1935+1616	40.6174	3.16151×10^{-24}	0.210985
J1937+2544	37.0187	5.19088×10^{-24}	0.301413
J1939+2134	76.5964	5.27885×10^{-26}	0.0037706
J1941-2602	38.8781	4.24401×10^{-24}	0.26523
J1944+0907	39.8356	6.16328×10^{-24}	0.399491
J1946-2913	42.4317	8.50239×10^{-24}	0.60585
J1946+1805	64.8701	1.3907×10^{-24}	0.099336
J1948+3540	40.2965	3.1063×10^{-24}	0.204849
J1952+3252	38.3669	6.99324×10^{-24}	0.428452

TABLE II: results of full calculation of h_c , f_c and S/N .

Jname	f_c	h_c	S/N
\hat{A}	[Hz]	\hat{A}	\hat{A}
J1954+2923	45.8579	1.06684×10^{-23}	0.762031
J1955+2908	43.7264	9.59627×10^{-25}	0.0685448
J1955+5059	40.8668	1.40886×10^{-23}	0.948881
J1959+2048	36.7592	9.00599×10^{-24}	0.517451
J2002+4050	41.0534	3.17817×10^{-24}	0.215521
J2004+3137	40.3195	2.74782×10^{-24}	0.181364
J2013+3845	35.0351	1.2161×10^{-23}	0.650212
J2018+2839	67.6517	9.09648×10^{-25}	0.0649749
J2019+2425	43.7666	5.66758×10^{-24}	0.404827
J2022+2854	38.4464	6.63234×10^{-24}	0.407605
J2022+5154	41.1168	3.41183×10^{-24}	0.231902
J2023+5037	36.6147	6.76838×10^{-24}	0.386596
J2046-0421	36.5212	3.44972×10^{-24}	0.196239
J2046+1540	37.6523	4.05443×10^{-24}	0.241493
J2048-1616	38.8761	3.17922×10^{-23}	1.9867
J2051-0827	67.0076	7.40902×10^{-25}	0.0529216
J2055+2209	57.4892	1.00494×10^{-24}	0.0717813
J2055+3630	41.9797	1.10321×10^{-24}	0.0773579
J2108+4441	44.3737	9.36083×10^{-25}	0.0668631
J2113+2754	39.1337	1.56216×10^{-23}	0.985915
J2113+4644	38.4549	3.59792×10^{-24}	0.221191
J2116+1414	37.9948	3.80432×10^{-24}	0.229695
J2124-3358	53.7137	1.10886×10^{-23}	0.792045
J2129+1210A	36.6794	1.3541×10^{-24}	0.0775484
J2129+1210B	42.2722	6.54473×10^{-25}	0.0463727
J2129+1210C	37.31	1.08497×10^{-24}	0.0637445
J2129-5721	43.8083	2.01653×10^{-24}	0.144038
J2145-0750	66.379	2.02952×10^{-24}	0.144966
J2149+6329	40.4712	4.24225×10^{-24}	0.281582
J2150+5247	36.9824	2.51365×10^{-24}	0.145743
J2157+4017	40.3436	4.42204×10^{-24}	0.292128
J2219+4754	39.1588	8.63068×10^{-24}	0.545228
J2225+6535	41.5695	4.25672×10^{-23}	2.94121
J2229+6205	37.6982	2.82253×10^{-24}	0.168426
J2229+2643	41.5673	4.51013×10^{-24}	0.311606
J2235+1506	43.6668	4.51705×10^{-24}	0.322647
J2257+5909	41.3007	4.20562×10^{-24}	0.287776
J2305+3100	39.1606	5.3719×10^{-24}	0.339384
J2308+5547	37.1242	4.60111×10^{-24}	0.26831
J2313+4253	43.4977	5.53556×10^{-24}	0.395397
J2317+1439	51.393	1.6924×10^{-24}	0.120886
J2321+6024	37.8303	5.16906×10^{-24}	0.31007
J2322+2057	44.9277	6.10354×10^{-24}	0.435967
J2326+6113	39.7623	4.82672×10^{-24}	0.311996
J2330-2005	37.0468	2.29858×10^{-23}	1.33621
J2337+6151	40.4429	2.95763×10^{-24}	0.196108
J2354+6155	38.8978	6.1822×10^{-24}	0.386652

V. COMPUTING DETECTABILITY OF GW FROM RAPs

One can discuss the detectability of the GW (burst) signal of the rise fling of galactic RAPs by using the *matching filter* technique. This procedure is based on

the definition of the *signal-to-noise ratio* (SNR), which is a quantity used as a criterium of detectability of a GW signal. The SNR depends on the features in the GW waveform of the process, the orientation of the source with respect to the GW interferometer (observer) and also on the source direction. It also depends on the total energy per unit frequency, $dE/df(f)$ (the GW energy spectrum at the source), that is carried away from the source by the GW, and on the distance to the source D_* . Here f is the average GW frequency for a given signal. Because of this angular dependence, the SNR is usually defined as

$$SNR = \langle \rho^2 \rangle = \frac{2}{5\pi^2 D_*^2} \int_0^\infty \frac{1}{f^2 S_h(f)} \frac{dE}{df} f df. \quad (8)$$

Symbol $\langle \rangle$ refers to an average of SNR square for all the directions (angles) to the GW source. In other words, it is obtained from the average *rms* of the amplitudes of the GW signals for different orientation of the source and the interferometer. In our computations above in Section III we applied this definition to estimate the S/N ratio given in Table II. As the attentive reader may notice, in what follows we shall use an equivalent definition of the SNR to quantify the detectability of RAPs GW signals in the context of the formalism of Ref.[19]

To complete this brief discussion on the SNR, we collect below the power-laws that according to most of the experimental studies with GW interferometers are what better describe the interferometer noise in each band of the spectrum. To this purpose, it is defined the dimensionless quantity: $h_{rms}(f) \equiv \sqrt{f S_h(f)}$, wherein $S_h(f)$ is the interferometer noise spectral density. Thus, the strain sensitivity for each frequency band is given by

$$h_{rms}(f) = \begin{cases} \infty, & f < f_s, \\ h_m (\alpha f / f_m)^{-3/2}, & f_s \leq f < f_m / \alpha, \\ h_m, & f_m / \alpha \leq f < \alpha f_m, \\ h_m [f / (\alpha f_m)]^{3/2}, & \alpha f_m < f. \end{cases} \quad (9)$$

Understanding these laws is straightforward if one recalls that the interferometer noise curves depend basically on four parameters:

- The threshold frequency f_s : below of it the noise grows almost asymptotically. For detectors on Earth the noise source is the seismic gradients
- The frequency f_m , centered in the almost flat part of the noise spectrum
- A critical amplitude h_m , which is the minimum value of $h_{rms}(f)$
- And the dimensionless parameter α , which determines the width of the flat band of the noise curve

For instance, for Advanced LIGO the following set of parameters is estimated (see E. E. Flanagan and S. A. Hughes, [Phys. Rev. D 57, 8 (1998)])

$$\text{LIGO Advanced} \begin{cases} f_s = 10 \text{ Hz} \\ f_m = 68 \text{ Hz} \\ \alpha = 1.6 \\ h_m = 1.4 \times 10^{-23} \end{cases} . \quad (10)$$

Therefore, to know whether the RAPs GW signals can be effectively detected by the currently operative interferometric detectors LIGO, VIRGO, GEO-600, etc., one needs to compute the signal-to-noise ratio with respect to the strain sensitivity of these instruments. (We refer to this procedure as *calibration*). In order to do that we need first to compute the frequency at which the largest part of the GW emission is expected to take place. This is the so-called characteristic frequency f_c , which is dependent on the detector design properties.

Should the detector have a power spectral density $S_h(f)$, have the characteristic frequency to be obtained from the frequency first moment of the time-dependent GW amplitude $h(t)$, i. e.,

$$f_c \equiv \left(\int_0^\infty \frac{\langle |\tilde{h}(f)|^2 \rangle}{S_h(f)} f df \right) \left[\int_0^\infty \frac{\langle |\tilde{h}(f)|^2 \rangle}{S_h(f)} df \right]^{-1}, \quad (11)$$

where $\langle \tilde{h}(f) \rangle$ is the Fourier transform of $h(t)$ [32], and the symbol $\langle \rangle$ stands for an average over randomly distributed angles of $h(f)$, and it can be approximated as $\langle |\tilde{h}(f)|^2 \rangle = |\tilde{h}(f)|^2$.

The characteristic frequency f_c is strictly related to the characteristic amplitude h_c , which is the physical quantity associated to the GW pulse $h(t)$ to be detected by a given instrument. It can be computed as

$$h_c(f_c) \equiv \left(3 \int_0^\infty \frac{S_h(f_c)}{S_h(f)} \langle |\tilde{h}(f)|^2 \rangle f df \right)^{1/2}. \quad (12)$$

In this way we take \tilde{h} in the following form (see Ref.[18, 19])

$$|\tilde{h}|^2 = \frac{(\Delta h_m)}{8\pi^4 f^4 t_m^2} (1 - \cos(2\pi t_m f)). \quad (13)$$

Here t_m defines the rise time of the memory of the signal. This equation is obtained from the Eq.(7) given above. Thus, Eq.(13) is the Fourier transform of the GW waveform, where Δh is given by (after average over angles in Eq.(7))

$$\Delta h_m = \frac{4G\beta^2\gamma M_\star}{c^2 D_\star} \quad (14)$$

with G the universal constant of gravitation, γ Lorentz factor, M_\star star mass, D_\star distance to Earth, and $\beta^2 = |\vec{V}|^2/c^2$.

Therefore, the signal-to-noise ratio S/N is now computed using the relation

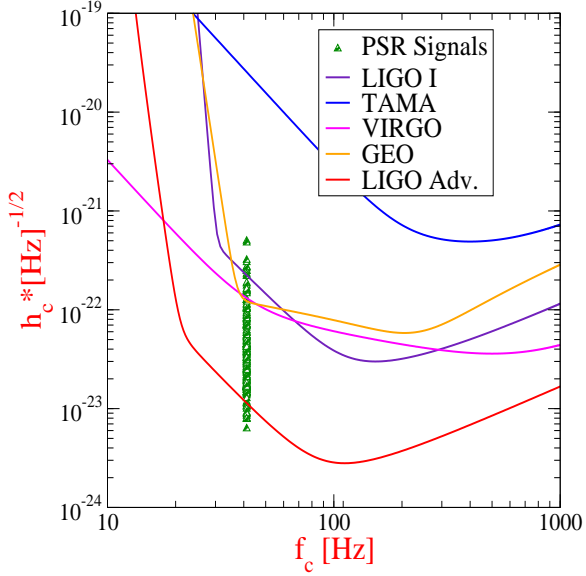
$$\frac{S}{N} = \frac{h_c(f_c)}{h_{rms}(f_c)} \quad (15)$$

where $h_{rms}(f_c) = [f_c S_h(f_c)]^{1/2}$ is the average amplitude of the interferometer spectral noise at the characteristic frequency.

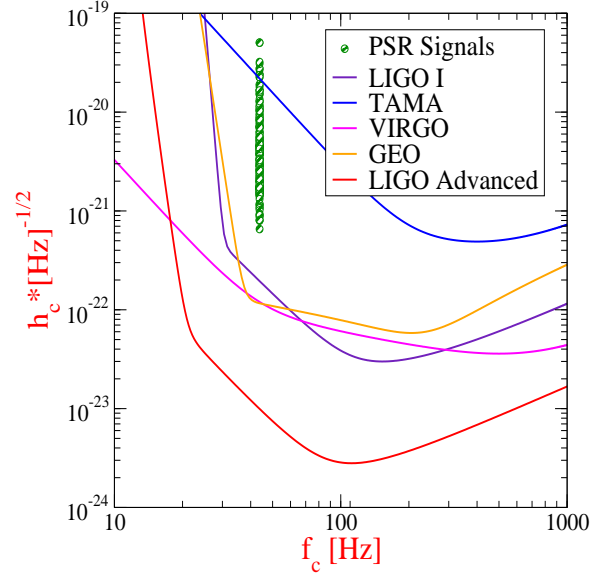
Guided by Table-IV, this allows us to compute the characteristic amplitude of the GW burst released during the short rise time of acceleration of each RAP for which those parameters are estimated. Since we are using only the transversal velocity of the pulsars, then we set $\theta \simeq 90^\circ$ in our calculations below. Our main results are presented in Figs.(4(a), 4(b), 5(a)). Those Figures compare the GW signals from individual RAPs with the expected sensitivities of LIGO I, its projected advanced configuration LIGO II, VIRGO, GEO-600, and TAMA-300 observatories.

At this stage, a note of caution to the attentive reader is needed. It regards with the appearance of the noise curves of TAMA, GEO and VIRGO GW observatories in figures from 4 through 9, in addition to the noise curves for LIGO I and LIGO Advanced, despite that the calibration of the expected signals in those figures (symbol: triangles, circles, etc.) is performed exclusively with respect to LIGO I and LIGO Advanced, independently. First, the reader must keep in mind that the position of those points in the diagram h_c vs. f_c will change when the calibration of the expect GW strain is performed with respect to the noise curve of a different detector, say TAMA, VIRGO, etc.. For instance, compare Fig.4(a) and Fig.5(a) which are calibrated for LIGO Advanced and LIGO I, respectively. Second, thinking on the benefit of the Scientific Community operating observatories like TAMA, GEO and VIRGO, those noise curves are included having in mind the expectation that such detectors might gain more sensitivity in both frequency band and amplitude so as to be able to catch the GW signals produced by Milky Way RAPs.

Finally, but not to the end, a direct interpretation of all the h_c vs. f_c diagrams in figures from 4 through 9 is that, exception done for the TAMA-300 GW detector, the signals (points) plotted in those figures appear to be not very much sensitive to the noise curves of the instruments LIGO I, LIGO Advanced, VIRGO and GEO-600. This feature justifies to include those noise curves in such figures.

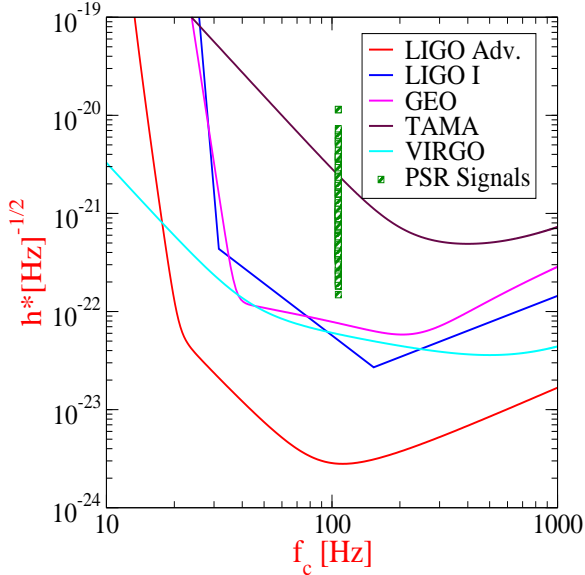


(a) LIGO I, LIGO Advanced, TAMA, VIRGO and GEO600 strain sensitivities and the h_c and f_c characteristics of the GW signal produced by each of the 212 pulsars calibrated with respect to LIGO Advanced, for parameters $a = 10^4 \text{ km s}^{-2}$ and $V_{\text{kick}} \sim 10^4 \text{ km s}^{-1}$.



(b) Idem as Fig.(4(a)), but now for parameters $a = 10^6 \text{ km s}^{-2}$ and $V_{\text{kick}} \sim 10^4 \text{ km s}^{-1}$, calibrated with respect to Advanced LIGO. It is possible to see that these signals have high enough chance to be detected.

FIG. 4: Color Online. Pulsar GW signals for different parameters a and V_{kick} . (a), (b)



(a) Idem as Fig.(4(a)), but now for parameters $a = 10^6 \text{ km s}^{-2}$ and $V_{\text{kick}} \sim 10^4 \text{ km s}^{-1}$, and calibrated against LIGO I. Clearly also these signals might be detected

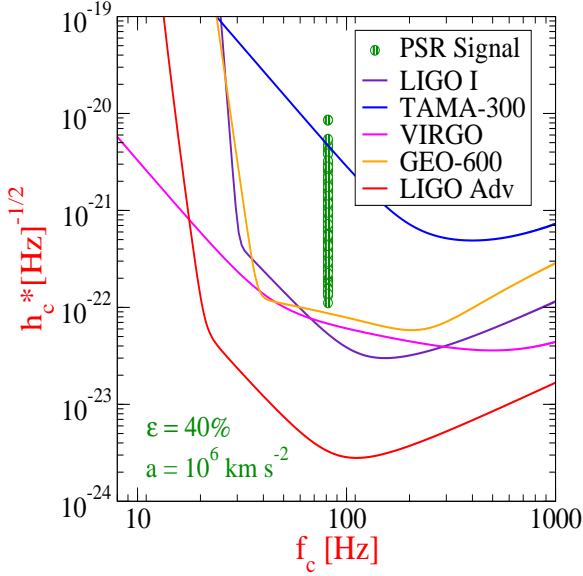
FIG. 5: Color Online. Pulsar GW signals for different parameters a and V . (c)

VI. MORE REALISTIC ANALYSIS OF GW EMISSION FROM RAPS

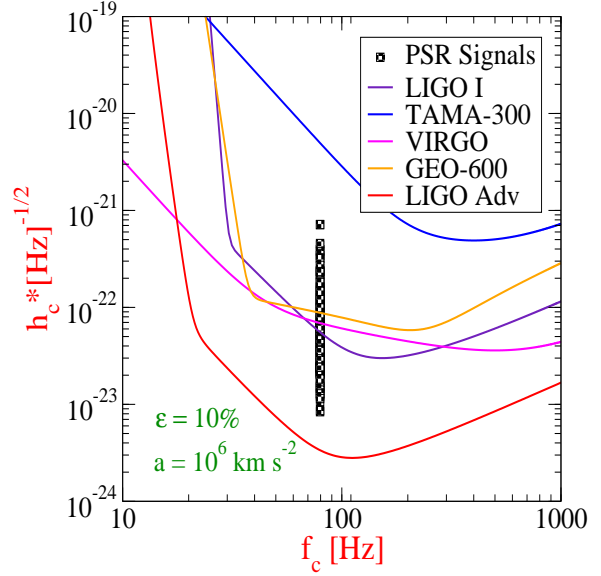
We can start with by recalling both the inertia (which is large for a neutron star progenitor) and linear momentum conservation laws, which should dominate the physics of the SN explosion that gives the kick to the neutron star. Thus, one can write

$$M_{SN}V_{SN} = M_{NS}V_{NS} - M_{RSN}V_{RSN}, \quad (16)$$

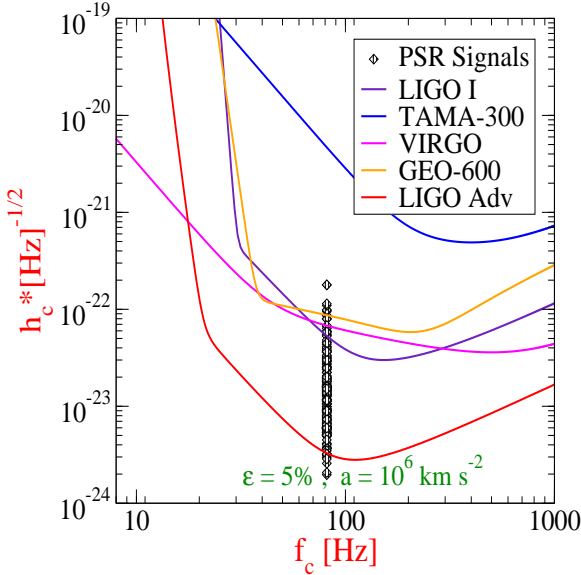
where M_{SN} , M_{NS} , and M_{RSN} are the SN, neutron star, and ejected material mass, respectively. Be aware of the role of the “-” signal in front of the term for the ejected material. It is responsible for a correct description of the physics at the explosion. Without it, one would obtain imaginary values for the searched parameter V_{NS} . Now, by assuming parameters of a typical progenitor star $M_{SN} = 10 M_{\odot}$, $V_{SN} = 15 \text{ km s}^{-1}$, $M_{NS} = 1.4 M_{\odot}$ for a canonical neutron star, and for the material in the ejected envelope $M_{RSN} = 8.6 M_{\odot}$, and expansion velocity $V_{RSN} = 3000 \text{ km s}^{-1}$ (see Table-IV), one obtains that the kick at birth velocity reads: $V_0 = V_{\text{kick}} \sim 10^4 \text{ km s}^{-1}$ (compare to velocities taken from ATNF in Fig.1(c)). The discrepancy between them will be briefly discussed below.



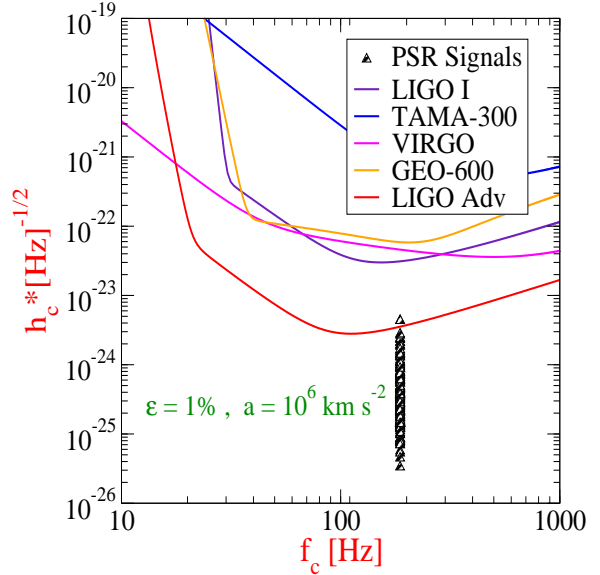
(a) Efficiency case $\epsilon = 0.40$ for parameters $a = 10^6 \text{ km s}^{-2}$ and $V_{\text{kick}} \sim 10^4 \text{ km s}^{-1}$, calibrated against LIGO Advanced.



(b) Efficiency case $\epsilon = 0.10$ for parameters $a = 10^6 \text{ km s}^{-2}$ and $V_{\text{kick}} \sim 10^4 \text{ km s}^{-1}$, calibrated against LIGO Advanced.



(c) Efficiency case $\epsilon = 0.05$ for parameters $a = 10^6 \text{ km s}^{-2}$ and $V_{\text{kick}} \sim 10^4 \text{ km s}^{-1}$, calibrated against LIGO Advanced.



(d) Efficiency case $\epsilon = 0.01$ for parameters $a = 10^6 \text{ km s}^{-2}$ and $V_{\text{kick}} \sim 10^4 \text{ km s}^{-1}$, calibrated against LIGO Advanced.

FIG. 6: Color Online. Pulsar GW signals for parameters: $a = 10^4 \text{ km s}^{-2}$ and $V_{\text{kick}} \sim 10^4 \text{ km s}^{-1}$

A. Case a: Centered kick $V = V_{\text{kick}}$ and $\epsilon = 1$

We first consider that the whole energy obtained from the conservation law discussed above goes into the pulsar kick, imparting to it no rotation at all. This is a very idealistic situation. Nonetheless, it gives us an idea on the potential detectability of those GW signals from the flinging of a pulsar out of the SN cocoon. In other words,

in this first approach we assume that the efficiency, ϵ , that relates the effective RAP velocity V (which enters the calculation of h_c) and the kick speed V_{kick} is $\epsilon = 1$ (In the other cases analyzed below these velocities will be related through the expression: $V = \epsilon V_{\text{kick}}$).

TABLE III: ATNF sample of pulsars having 2-Dim speed greater than 10^3 km s^{-1} . The current high velocities suggest that a much higher speed was imparted at the kick at birth.

Jname	DIST	VTrans
	[kpc]	[km s^{-1}]
J0525+1115	7.68	1101.985
J1509+5531	2.41	1104.013
J1824-1945	5.20	2482.989
J1829-1751	5.49	3945.954
J2013+3845	13.07	2521.130
J2149+6329	13.65	1113.385
J2225+6535	2.00	1729.770
B2011+38	????	1624.0
B2224+65	????	1608.0
B1830-1945	5.20	740.0
*RX J0822-4300	2.0	1600.0

*Ref. P. F. Winkler & R. Petre, *Direct measurement of neutron star recoil in the Oxygen-rich supernova remnant Puppis A*, Ap.J. 670, 635 (2007)

1. *Fling with $a = 10^4 \text{ km s}^{-2}$, $V_{\text{kick}} = 10^4 \text{ km s}^{-1}$*

Based on the dynamical analysis presented in the Section-III, we suppose here that the short rise time kick imparts to the pulsar an acceleration $a = 10^4 \text{ km s}^{-2}$, and a birth velocity $V_{\text{kick}} = 10^4 \text{ km s}^{-1}$. The GW signal obtained for these parameters is presented in Figs.(4(a), 4(b)).

2. *Fling with $a = 10^6 \text{ km s}^{-2}$, $V_{\text{kick}} = 10^4 \text{ km s}^{-1}$*

Now one can take a step further and consider that the birth acceleration is actually more larger than the one currently inferred from the RAPs galactic parameters. Several physical mechanisms can act together to impart an acceleration as large as $a = 10^6 \text{ km s}^{-2}$, see for instance Refs.[23, 24, 26], and references therein. Such a large thrust can be estimated as $a \simeq V_{\text{kick}}/\Delta T_{\text{mech}}$, where ($10^{-1} \lesssim \Delta T_{\text{mech}} \lesssim 10^{-3}$) s, depending on the specific mechanism driving the fling. The GW signal obtained for these parameters is presented in Fig.(5(a)).

B. Case b: Off-centered kick

Finally, we analyze the most astrophysically realistic kicks at birth: a situation where the pulsar receives both a translational and a rotational kick. In this case, the energy transferred to the translational kick can be parameterized by an efficiency ϵ , which ranges from 0 to 1. Of course, this efficiency represents our difficulty in explaining how a specific kick mechanism becomes the kick driver. The remaining energy is

supposed to be expended in making the pulsar to spin. This parametrization can be translated into a power-law relationship between the GW amplitude, h , and the efficiency, ϵ , of energy conversion into pulsar kick, which has the form:

$$h \propto \epsilon^2. \quad (17)$$

This relation stems from the quadratic dependence of the GW amplitude with the β parameter appearing in Eq.(7) above. In this way, one can recover the whole spectrum of RAPs velocities as observed today and listed in ATNF catalog. To exemplify, we compute signals for values of $\epsilon = 0.01, 0.05, 0.10$, and 0.40 , which can reproduce the set of velocities $V_{\text{kick}} = 100 \text{ km s}^{-1}$, $V_{\text{kick}} = 500 \text{ km s}^{-1}$, $V_{\text{kick}} = 10^3 \text{ km s}^{-1}$, and $V_{\text{kick}} = 4 \times 10^3 \text{ km s}^{-1}$, as shown in Fig.-(1(c)). For this case, the results are presented in Figs.(6, 7, 8, 9). To the end of the paper a brief discussion on the pulsar periods provided by the ATNF catalog is given.

1. *Efficiency $\epsilon = 0.05$*

The following figures illustrate the results obtained for this efficiency: Fig.(7(c)) with $a = 10^6 \text{ km s}^{-2}$ and Fig.(6(c)) with $a = 10^4 \text{ km s}^{-2}$ for advanced. Fig.(8(c)) with $a = 10^6 \text{ km s}^{-2}$ and Fig.(9(c)) with $a = 10^4 \text{ km s}^{-2}$ para LIGO I.

2. *Efficiency $\epsilon = 0.10$*

The following figures illustrate the results obtained for this efficiency: Fig.(7(b)) with $a = 10^6 \text{ km s}^{-2}$ and Fig.(6(b)) with $a = 10^4 \text{ km s}^{-2}$ for Advanced LIGO. Fig.(9(b)) with $a = 10^6 \text{ km s}^{-2}$ and Fig.(8(b)) with $a = 10^4 \text{ km s}^{-2}$ for LIGO I.

3. *Efficiency $\epsilon = 0.40$*

The following figures illustrate the results obtained for this efficiency: Fig.(7(a)) with $a = 10^6 \text{ km s}^{-2}$ and Fig.(6(a)) with $a = 10^4 \text{ km s}^{-2}$ for Advanced LIGO. Fig.(9(a)) with $a = 10^6 \text{ km s}^{-2}$ and Fig.(8(a)) with $a = 10^4 \text{ km s}^{-2}$ for LIGO I.

VII. DISCUSSION AND CONCLUSIONS

A. Computed rotation periods vs. Periods of ATNF sample of RAPs with $V = 400 - 500 \text{ km s}^{-1}$

To the end, in order to make our analysis self-consistent we next discuss the relation between the translational speed and rotation frequency of ATNF

TABLE IV: High expansion speeds of CaII and SiII lines of the ejected material in some supernovae. Data taken from A. Balastegui, P. Ruiz-Lapuente, J. Méndez, G. Altavilla, M. Irwin, K. Schahmaneche, C. Balland, R. Pain and N. Walton. arXiv: astro-ph/0502398v1 21 Feb 2005

Event	CaII Expansion Speed [km s ⁻¹]	SiII Expansion Speed [km s ⁻¹]	Days after maximum [days]
SN 2002li	17200± 500		-7
SN 2002lj	12300± 300	8900± 300	7
SN 2002lp	13800± 900	10400± 400	3
SN 2002lq	18900± 1400		-7
SN 2002lr	12800± 300	8600± 400	10
SN 2002lk		14500± 500	-5

pulsars. To do this, we select, as an example, the 3-D average pulsar velocity as determined by Hobbs et al. [10] (see Table-V). On this basis we determine the theoretical rotation periods that one could expect to find for that velocity sample if is factual that most of the explosion energy, as inferred from the momentum conservation law in Eq.(16), goes into the pulsar rotation as discussed above. (Of course we compare with the actual periods measured by the ATNF surveys). Hence the torque applied to the just-born neutron star reads

$$\tau \sim \frac{V}{2E_k} \frac{\frac{2}{5}M_{NS}R_{NS}^2}{d_l} \quad (18)$$

where E_k is the kinetic energy of each velocity chosen for the present analysis, V pulsar velocity, $M_{NS} = 1.4 M_{\odot}$, $R_{NS} = 20$ km and $d_l = 25$ km are the neutron star mass, radius and torque lever. Thus, for $R_{NS} = 20$ km and velocity $V = 350$ km s⁻¹ we obtain $p = 0.0182$ s, while for $V = 433$ km s⁻¹ one gets $p = 0.0182$ s. Meanwhile, for $R_{NS} = 30$ km and $V = 350$ km s⁻¹ we have $p = 0.0411$ s, while for $V = 433$ km s⁻¹ one gets $p = 0.0332$ s.

One can then compare these results with those presented in Table-V. It appears that the theoretical prediction is about an order of magnitude smaller (much shorter periods) than the observed, and measured by the ATNF surveys. This discrepancy may suggest that

- 1) perhaps a large part of the initial rotational energy is dissipated by processes as differential rotation or magnetic braking, especially if processes as the magneto-rotational instability[27] indeed drives a large class of supernova explosions [22].
- 2) it may also happen that convection and neutron fingers also becomes highly effective dissipative processes, thus reducing the pulsar initial spin to

the level that we are currently finding in pulsar surveys.

In summary, from astronomical statistics the number of observed Galactic RAPs is definitely much larger than the corresponding to relativistic NS-NS binaries. The typical lifetime of canonical pulsars is ~ 10 Myr, which is defined as the duration of the radio emitting phase for objects with $B \sim 10^{12}$ G, or the time needed for the pulsar to emit less radiation or being entirely turned off. Hence, with a statistical Galactic rate of SNe, and the likely fling out rate of just-born pulsars, of about 1 per every 30-300 years, one expects that the GW signal of the kick at birth be observable as aftermath of the SN core collapse. In other words, the RAP GW signal may become a benchmark for looking for GW signals from the SN gravitational implosion. Besides, if the GW signal from the kick to a RAP were detected, for instance, from a source inside a globular, or from either an open star cluster [16], or a binary system harboring a compact star, such an observation might turn these RAPs the most compelling evidence for the existence of Einstein's gravitational waves.

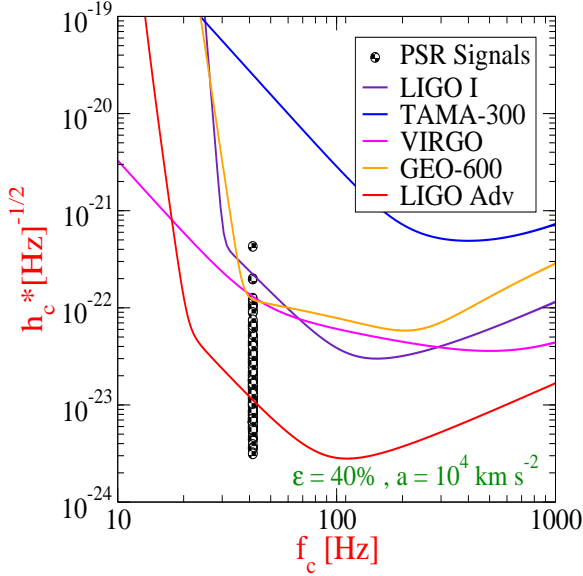
We conclude by stating that the detection with advanced LIGO-type interferometers of individual GW signals from the short rise fling of Galactic RAPs is indeed possible.

Acknowledgments

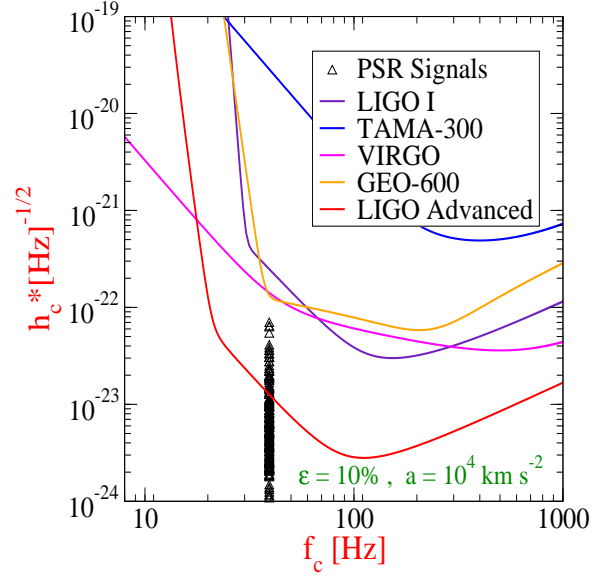
HJMC thanks Prof. José A. de Freitas Pacheco (OCA-Nice) for the hospitality during the initial development of this idea. Dr. Sebastien Peirani (OCA-Nice), Marcelo Perantonio (CBPF-Rio de Janeiro), and folks as Dr. Eric Lagadec (OCA-Nice) are also thanked. HJMC is fellow of Fundação de Amparo à Pesquisa do Estado do Rio de Janeiro (FAPERJ), Brazil.

[1] R. N. Manchester, G. B. Hobbs, A. Teoh, M. Hobbs, *The ATNF pulsar catalogue* (Australia, CSIRO,

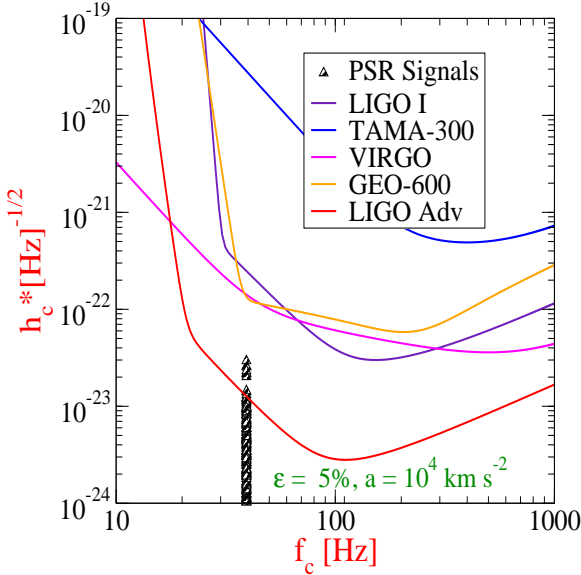
Epping), *Astron. J* 129, 1993-2006 (2005), e-Print:



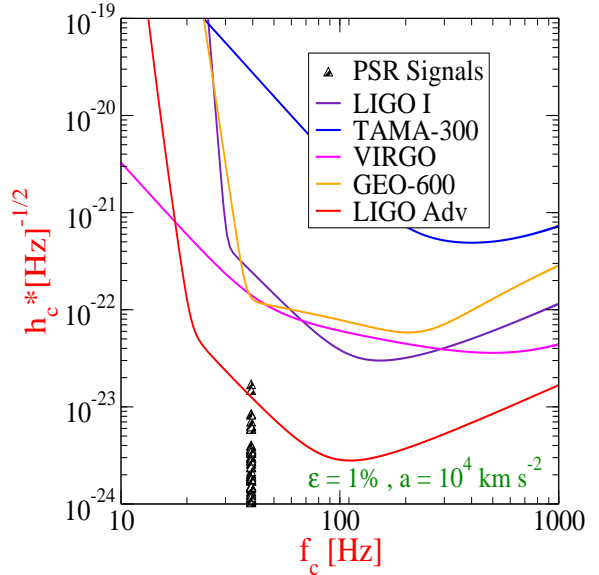
(a) Efficiency case $\epsilon = 0.40$ for parameters $a = 10^4$ km s $^{-2}$ and $V_{\text{kick}} \sim 10^4$ km s $^{-1}$, calibrated against LIGO Advanced.



(b) Efficiency case $\epsilon = 0.10$ for parameters $a = 10^4$ km s $^{-2}$ and $V_{\text{kick}} \sim 10^4$ km s $^{-1}$, calibrated against LIGO Advanced.



(c) Efficiency case $\epsilon = 0.05$ for parameters $a = 10^4$ km s $^{-2}$ and $V_{\text{kick}} \sim 10^4$ km s $^{-1}$, calibrated against LIGO Advanced.

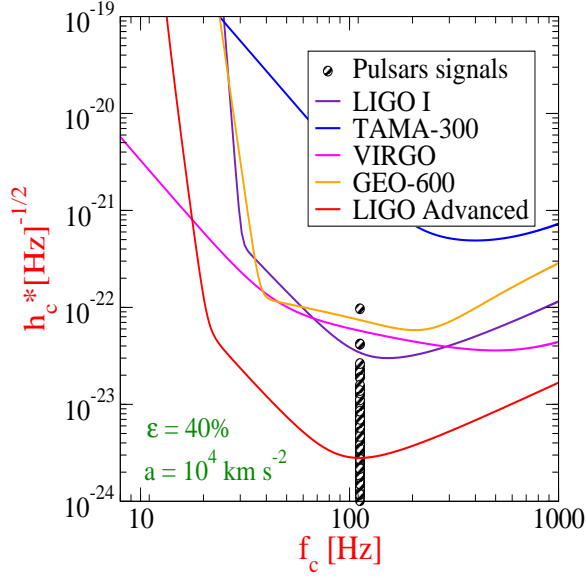


(d) Efficiency case $\epsilon = 0.01$ for parameters $a = 10^4$ km s $^{-2}$ and $V_{\text{kick}} \sim 10^4$ km s $^{-1}$, calibrated against LIGO Advanced.

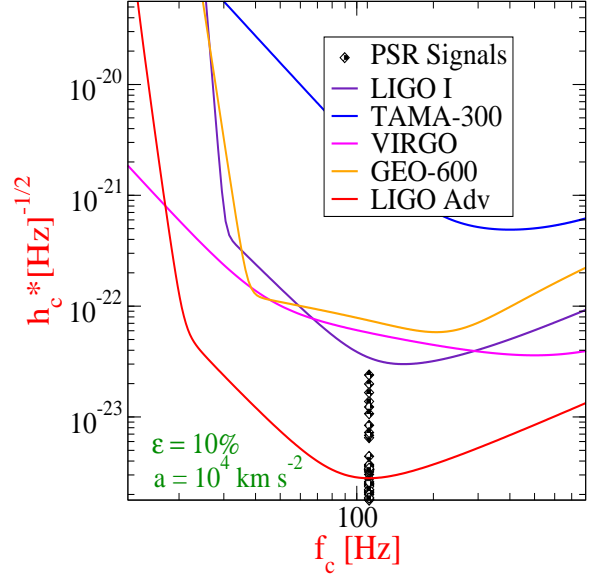
FIG. 7: Color Online. Pulsar GW signals for parameters: $a = 10^4$ km s $^{-2}$ and $V_{\text{kick}} \sim 10^4$ km s $^{-1}$

astro-ph/0412641
 [2] Lorimer, D.R., et al., MNRAS 263, 403 (1993).
 [3] Lyne, A.G. & Lorimer, D.R., 1994, Nature 369, 127,
 [4] Z. Arzoumanian, D. Chernoff, J. M. Cordes, Astrophys. J. 568, 289 (2002)
 [5] Spruit, H. & Phinney, S. E., Nature 393, 139 (1998) .
 [6] V. B. Braginsky, K. S. Thorne, Nature 327., 123-125 (1987)
 [7] J. M. Cordes, D. F. Chernoff, Astrophys. J. 505, 315-338

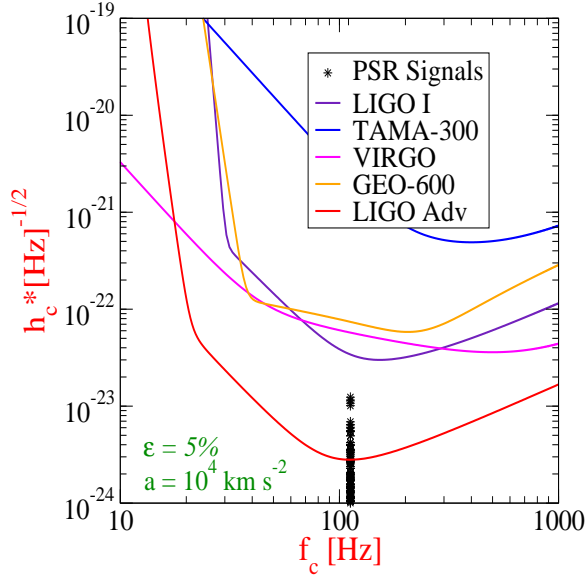
(1998)
 [8] D. Chakrabarty, S. E. Thorsett, Astrophys. J. 512, 288-299 (1998)
 [9] R. N. Manchester, G. B. Hobbs, A. Teoh, M. Hobbs, 'The ATNF Pulsar Catalog'. Report astro-ph/0412641 (2004). The ATNF web-site is found via the URL link <http://www.atnf.csiro.au/research/pulsar/psrcat>
 [10] G. Hobbs et al., MNRAS 360, 974 (2005)
 [11] B. Abbott et al., LIGO Science Collaboration,



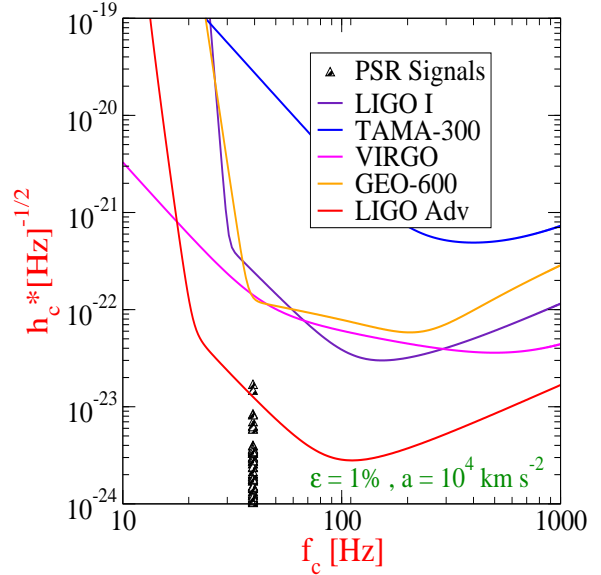
(a) Efficiency case $\epsilon = 0.40$ for parameters $a = 10^4 \text{ km s}^{-2}$ and $V_{\text{kick}} \sim 10^4 \text{ km s}^{-1}$, calibrated against LIGO I.



(b) Efficiency case $\epsilon = 0.10$ for parameters $a = 10^4 \text{ km s}^{-2}$ and $V_{\text{kick}} \sim 10^4 \text{ km s}^{-1}$, calibrated against LIGO I.



(c) Efficiency case $\epsilon = 0.05$ for parameters $a = 10^4 \text{ km s}^{-2}$ and $V_{\text{kick}} \sim 10^4 \text{ km s}^{-1}$, calibrated against LIGO I.



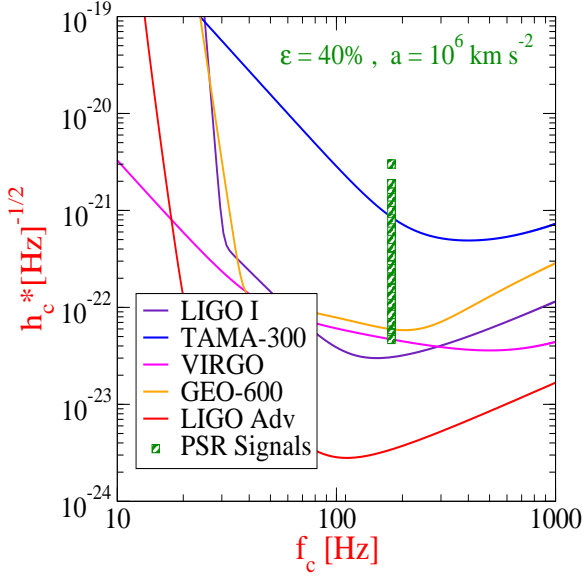
(d) Efficiency case $\epsilon = 0.01$ for parameters $a = 10^4 \text{ km s}^{-2}$ and $V_{\text{kick}} \sim 10^4 \text{ km s}^{-1}$, calibrated against LIGO I.

FIG. 8: Pulsar GW signals for parameters: $a = 10^4 \text{ km s}^{-2}$ and $V_{\text{kick}} \sim 10^4 \text{ km s}^{-1}$

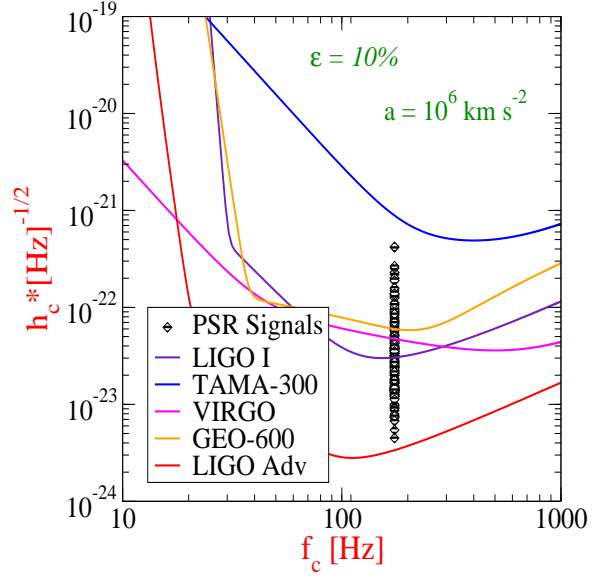
arXiv:0704.3368L

- [12] K. A. Postnov, L. Youngelson, Liv. Rev. Rel. 9, 6 (2006)
- [13] V. Kalogera et al. Phys. Rep. 442, 75 (2007)
- [14] Weisberg, J. M. Taylor, J. H., 2003. The Relativistic Binary Pulsar B1913+16. Conference Proceedings, Vol. 302. Held 26-29 August 2002 at Mediterranean Agronomic Institute of Chania, Crete, Greece. Edited by Matthew Bailes, David J. Nice and Stephen E. Thorsett. San Francisco: Astronomical Society of the Pacific, 2003. ISBN: 1-58381-151-6, p.93

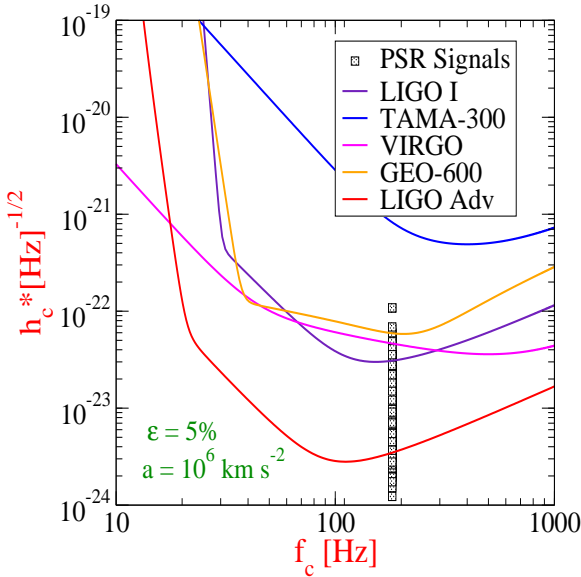
- [15] R. Wijnands and M. van der Klis, Nature 394, 344 (1998)
- [16] W.H.T. Vlemmings, S. Chatterjee, W.F. Brisken, T.J.W. Lazio, J.M. Cordes, S.E. Thorsett, W.M. Goss, E.B. Fomalont, M. Kramer, A.G. Lyne, S. Seagroves, J.M. Benson, M.M. McKinnon, D.C. Backer, R. Dewey, *Pulsar Astrometry at the Microarcsecond Level*. In the proceedings of the "Stellar End Products" workshop, 13-15 April 2005, Granada, Spain (for publication in MmSAI vol.77). arXiv:astro-ph/0509025
- [17] Coryn A. L. Bailer-Jones *Microarcsecond astrometry*



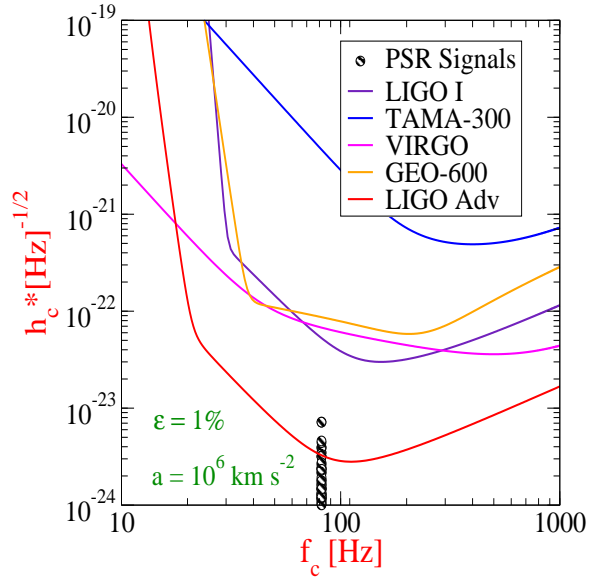
(a) Efficiency case $\epsilon = 0.40$ for parameters $a = 10^6 \text{ km s}^{-2}$ and $V_{\text{kick}} \sim 10^4 \text{ km s}^{-1}$, calibrated against LIGO I.



(b) Efficiency case $\epsilon = 0.10$ for parameters $a = 10^6 \text{ km s}^{-2}$ and $V_{\text{kick}} \sim 10^4 \text{ km s}^{-1}$, calibrated against LIGO I.



(c) Efficiency case $\epsilon = 0.05$ for parameters $a = 10^6 \text{ km s}^{-2}$ and $V_{\text{kick}} \sim 10^4 \text{ km s}^{-1}$, calibrated against LIGO I.



(d) Efficiency case $\epsilon = 0.01$ for parameters $a = 10^6 \text{ km s}^{-2}$ and $V_{\text{kick}} \sim 10^4 \text{ km s}^{-1}$, calibrated against LIGO I.

FIG. 9: Pulsar GW signals for parameters: $a = 10^6 \text{ km s}^{-2}$ and $V_{\text{kick}} \sim 10^4 \text{ km s}^{-1}$

with Gaia: *The Solar system, the Galaxy and beyond*. Invited paper at IAU Colloquium 196: Transits of Venus: New Views of the Solar System and Galaxy, Lancashire, England, United Kingdom, 7-11 Jun (2004) Submitted to IAU Symp. e-Print: astro-ph/0409531. See also O. Fors in *New observational techniques and analysis tools for wide field CCD surveys and high resolution astrometry* (2006). e-Print: astro-ph/0604150. Also see E. Fomalont, M. Reid, *Microarcsecond Astrometry using the SKA*, *New Astron. Rev.* 48, 1473-1482 (2004)

- [18] N. Sago, et al., *Phys. Rev. D* 70, 104012-1,104012-8 (2004).
- [19] B. Segalis, A. Ori, *Phys. Rev. D* 64, 064018 (2001)
- [20] H. J. Mosquera Cuesta and C. A. Bonilla Quintero, *The gravitational-wave background produced by the kick at birth of galactic run away pulsars*, (accompanying paper in preparation) (2007)
- [21] Jose A. de Freitas Pacheco, Tania Regimbau, S. Vincent, A. Spallicci *Int. J. Mod. Phys. D* 15:235-250 (2006). e-Print: astro-ph/0510727: *Expected coalescence rates of*

TABLE V: Selected sample from the ATNF catalog of pulsars having speeds between 350-500 km s⁻¹, and their corresponding periods.

#	JNAME	PERIOD [s]	VTRANS [km s ⁻¹]
1	J0255-5304	0.447708	381.648
2	J0538+2817	0.143158	401.682
3	J0543+2329	0.245975	377.151
4	J0837-4135	0.751624	364.772
5	J1300+1240	0.006219	350.637
6	J1645-0317	0.387690	417.022
7	J1803-2137	0.133617	351.252
8	J1902+0615	0.673500	368.086
9	J1941-2602	0.402858	351.027
10	J2048-1616	1.961572	355.328
11	J2113+2754	1.202852	386.791
12	J2219+4754	0.538469	375.304
13	J2305+3100	1.575886	373.546
14	J2326+6113	0.233652	433.576
15	J2354+6155	0.944784	357.846

ns-ns binaries for laser beam interferometers

- [22] A. Ud-Doula, J. Blondin, *The Magneto-Rotational Instability in Core-Collapse Supernovae*, American Physical Society, The 70th Annual Meeting of the Southeastern Section, November 6-8, 2003, Wilmington, North Carolina, MEETING ID: SES03, abstract #EB.009. See also S. Akiyama, J. C. Wheeler, D. L. Meier, and I. Lichtenstadt, AAS 199.9403 (2001); J. Craig Wheeler, *Rotation and Magnetic Fields in Supernovae and Gamma-ray Bursts*, American Physical Society, 47th Annual DPP Meeting, October 24-28 (2005), abstract #CZ2.002; P. Cerd n-Dur n, J. A. Font, H. Dimmelmeier, Astron. & Astrophys. 474, 169 (2007); L. Dessart, A. Burrows, E. Livne, C. Ott, *The Proto-neutron Star Phase of the Collapsar Model and the Route to Long-soft Gamma-ray Bursts and Hypernovae*, arXiv: 0710.5789 (2007); M. Shibata, Y. T. Liu, S. L. Shapiro, C. B. Stephens, PRD 74, 104026 (2006), *Magnetorotational collapse of massive stellar cores to neutron stars: Simulations in full general relativity*
- [23] Chris L. Fryer, Astrophys.J.601:L175-L178,2004. e-Print: astro-ph/0312265, *Neutron star kicks from asymmetric collapse.* See also, Aristotle Socrates, Omer Blaes, Aimee L. Hungerford, Chris L. Fryer Astrophys. J. 632: 531-562 (2005). e-Print: astro-ph/0412144, *The Neutrino bubble instability: A Mechanism for generating pulsar kicks*; Chris L. Fryer, Alexander Kusenko, Astrophys. J. Suppl. 163:335 (2006), e-Print: astro-ph/0512033, *Effects of neutrino-driven kicks on the supernova explosion mechanism*
- [24] Leonhard Scheck, K. Kifonidis, H.-Th. Janka, E. Mueller, *Multidimensional supernova simulations with approximative neutrino transport. 1. neutron star kicks and the anisotropy of neutrino-driven explosions in two spatial dimensions*, Submitted to Astron.Astrophys. e-Print: astro-ph/0601302. See also Hans-Thomas Janka, L. Scheck, K. Kifonidis, E. Muller, T. Plewa *Supernova asymmetries and pulsar kicks - Views on controversial issues*. e-Print: astro-ph/0408439
- [25] D. Lai (2004). In *cosmic explosions in three dimensions: asymmetries in supernovae and gamma-ray bursts*, eds. P. Hoflich, P. Kumar, J. C. Wheeler (Cambridge University Press, Cambridge), p. 276
- [26] Dong Lai, *Neutron star kicks and asymmetric supernovae*. e-Print: astro-ph/0012049. See also Chen Wang, Dong Lai, JinLin Han, Astrophys.J.639, 1007-1017 (2006). e-Print: astro-ph/0509484: *Neutron star kicks in isolated and binary pulsars: observational constraints and implications for kick mechanisms*
- [27] L. M. Ozernoy, B. V. Somov, Ap. S S 11, 264O(1971) *The Magnetic Field of a Rotating Cloud and Magneto-Rotational Explosions*
- [28] <http://www.atnf.csiro.au/research/pulsar/psrcat>
- [29] Notice that here we are assuming that the measured velocities are the very initial ones. That is, we are neglecting the effects of the gravitational potential of the galactic central distribution of mass, the bulge, which can affect the presently observed kinematics and energetics, especially, of young pulsars born near the galactic plane [7].
- [30] We stress that even if larger velocities were found in forthcoming pulsar surveys [7], this would not change significantly the picture here presented.
- [31] As above-mentioned the ATNF catalog contains data on pulsar velocities, V_* , distances, r_* and orientations (θ, ϕ) angles with respect to the line of sight.
- [32] The Fourier transform reads: $\tilde{h} = \int_{-\infty}^{\infty} e^{2\pi i f t} h(t) dt$